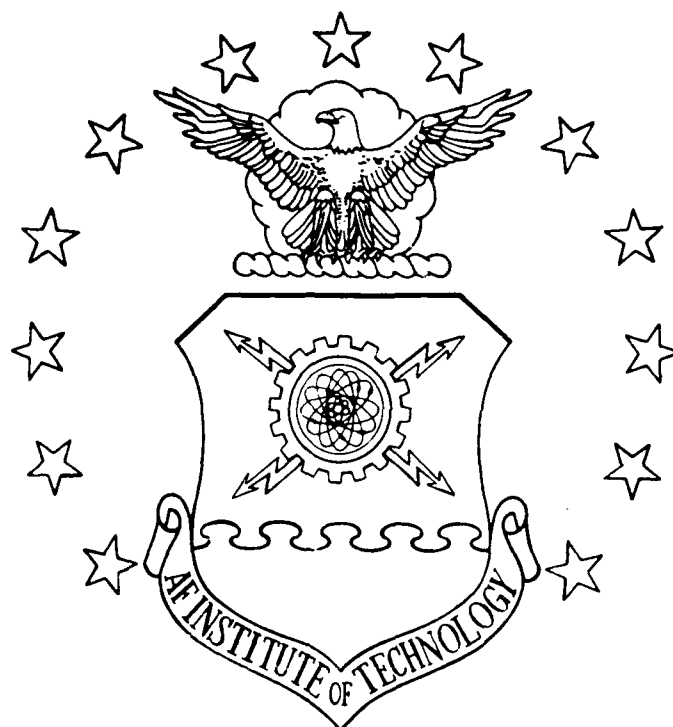


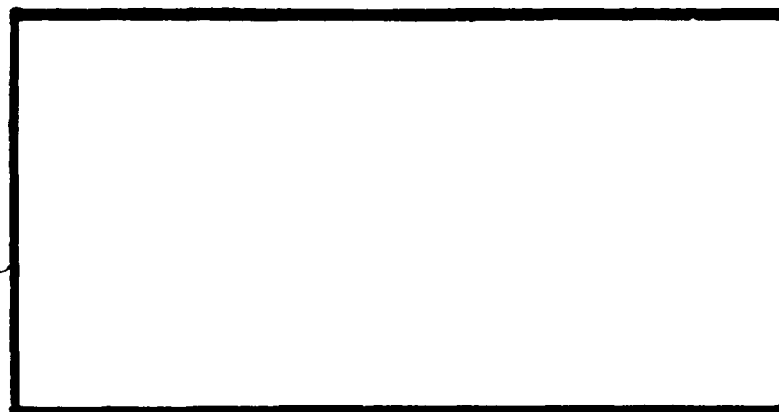
AD-A238 457



1



**DTIC**  
ELECTE  
JUL 22 1991  
**S D**



**DISTRIBUTION STATEMENT A**  
Approved for public release  
Distribution Unlimited

DEPARTMENT OF THE AIR FORCE  
AIR UNIVERSITY  
**AIR FORCE INSTITUTE OF TECHNOLOGY**

Wright-Patterson Air Force Base, Ohio

AFIT/GA/ENY/91M-01



EFFECTS OF COLOCATION AND NON-COLOLOCATION  
OF SENSORS AND ACTUATORS  
ON FLEXIBLE STRUCTURES

THESIS

W. C. LEE, Captain, USAF

AFIT/GA/ENY/91M-01

Approved for public release; distribution unlimited.



March 1991  
Effect of Colocation and  
Non-colocation of Sensors and Actuators  
on Flexible Structures

Master Thesis

W. C. Lee, Capt, USAF

Air Force Institute of Technology  
WPAFB, OH 45433-6583

AFIT/GA/ENY/91M-01

Approved for public release; distribution  
unlimited

This thesis compares the performance and robustness of colocated and non-colocated sensor/actuator pairs. Linear quadratic Gaussian and loop transfer recovery (LQG/LTR) procedures are used to design optimum controllers for three example problems. The first example is a single motion degree-of-freedom system having motion only about one axis. This type of system does not have any right half plane zeros for the non-colocated case; however, the thesis shows it behaves as a non-minimum phase system. The second example is a Bernoulli-Euler beam which does have RHP zeros. An optimum LQG/LTR controller can not improve the robustness of non-minimum phase systems; whereas, colocated systems are easy to stabilize and make robust with LTR. However, this thesis shows that non-colocated systems can achieve higher bandwidth and performance. So, each system has its own advantage.

control theory, flexible structures, actuators, LQG/LTR

133

unclassified

unclassified

unclassified

unlimited

AFIT/GA/ENY/91M-01

EFFECTS OF COLOCATION AND NON-COLOLOCATION  
OF SENSORS AND ACTUATORS  
ON FLEXIBLE STRUCTURES

THESIS

Presented to the Faculty of the School of Engineering  
of the Air Force Institute of Technology

Air University

In Partial Fulfillment of the  
Requirements for the Degree of  
Master of Science in Astronautical Engineering

W. C. Lee, B.S.C.E.

Captain, USAF

March 1991

Approved For	
1-15-1991	
1-15-1991	
1-15-1991	
1-15-1991	
By	
Date: 1-15-1991	
Approved For	
Date	Approved For
A-1	Spec. 001

Approved for public release; distribution unlimited.

### Acknowledgements

I wish to thank Mr Dan Malwitz of Contraves USA for providing the finite element model used in this thesis. He was very helpful in clarifying questions I had concerning finite element modeling and providing supporting materials. Another group who deserves much thanks is the people at Engineering Methods, Inc. of West Lafayette, Indiana. From Luanna Hellerger, Paul Hunckler and Dave Phillips to Dr. Charles Hunckler, I can not appreciate the amount of time and effort they took to assist me in getting ANSYS up and running. Also, Mr Bob Jurek and Mr Larry Falb at ASD's Scientific and Engineering Applications Division were very helpful in getting an account set up so I could use the commercial version of ANSYS for some of my computer runs. I also appreciate the contributions of the in-house people here at AFIT's computer support and Capt Howard Gans in getting ANSYS set up in our own laboratory. Finally, I need to thank Dr Patrick Sweeney and Mr Tom Davis from University of Dayton who provided the initial support in my using ANSYS as a research tool.

My deepest appreciation goes toward my thesis advisor, Dr Brad Liebst, for his motivation and support during this thesis effort. His patience and dedication to higher learning allowed me to leave AFIT with a feeling of accomplishment in

having learned a little about the new and exciting field of control engineering. I also appreciate the help of my thesis committee members, Capt Brett Ridgely, Lt Col Ron Bagley and Dr Curtis Spenny for their helpful advice and support in finishing my thesis. Of course, my wife, Myong Sook, deserves the most gratitude. Her endless patience during my long hours at the computer and in the laboratory is something few people could give. Her love and support got me through this project and AFIT.

W. C. Lee

## Table of Contents

Acknowledgements . . . . .	ii
List of Figures . . . . .	vi
List of Tables . . . . .	ix
Abstract . . . . .	x
I. Introduction . . . . .	1-1
II. Background . . . . .	2-1
2.1 Pole/Zero Patterns for the Colocated Systems	2-2
2.2 Pole/Zero Patterns for the Non-colocated Systems . . . . .	2-6
2.3 Three Element Lumped Mass Model . . . . .	2-8
2.3.1 Colocation . . . . .	2-13
2.3.2 Non-colocation . . . . .	2-17
III. Linear Quadratic Gaussian/Loop Transfer Recovery	3-1
3.1 LQG/LTR Theory . . . . .	3-1
3.2 Linear Quadratic Regulator . . . . .	3-2
3.3 Linear Quadratic Estimator . . . . .	3-4
3.4 Linear Quadratic Gaussian . . . . .	3-7
3.5 LQG Design On Three Element Model . . . . .	3-10
3.6 Loop Transfer Recovery . . . . .	3-16
3.6.1 Root Mean Square Response . . . . .	3-19
3.6.2 LTR With Non-minimum Phase Systems .	3-20
3.7 LTR On Three Element Model . . . . .	3-20
3.8 Step Response . . . . .	3-25
3.9 Conclusion . . . . .	3-26
IV. A Two Motion Degree of Freedom System . . . . .	4-1
4.1 Introduction . . . . .	4-1
4.2 Exact Solution of a Transverse Beam . . . . .	4-1

4.2.1	Modal Truncation and Its Effect on Zero Location . . . . .	4-5
4.3	Approximate Solution by Finite Element Method . . . . .	4-5
4.4	Ten Element Transverse Beam Example . . . . .	4-8
4.4.1	Model Reduction to Four Modes . . . . .	4-12
4.5	LQG/LTR Control Design on the Beam . . . . .	4-19
4.5.1	Step Response . . . . .	4-25
4.6	Conclusion . . . . .	4-26
V.	Finite Element Model of Contraves P52F Gimbals . . . . .	5-1
5.1	Finite Element Modeling . . . . .	5-1
5.2	LQG/LTR Control Design on the Gimbals . . . . .	5-8
5.3	Step Response . . . . .	5-13
5.4	Conclusion . . . . .	5-14
VI.	Conclusion and Recommendations . . . . .	6-1
6.1	Summary . . . . .	6-1
6.2	Contribution . . . . .	6-4
6.3	Recommendations for Further Study . . . . .	6-5
APPENDIX A:	LQG/LTR Design Results . . . . .	A-1
APPENDIX B:	ANSYS FEM Files . . . . .	B-1
APPENDIX C:	MATLAB Programs . . . . .	C-1
Bibliography	. . . . .	BIB-1
Vita	. . . . .	V-1

## List of Figures

Figure	Page
2.1 Alternating Poles and Zeros . . . . .	2-5
2.2 Three Element Lumped Mass Model . . . . .	2-8
2.3 Bode Plots of Colocated and Non-colocated Three Element Model . . . . .	2-12
2.4 Closed Loop System with Unity Feedback and Proportional Gain . . . . .	2-13
2.5 Colocation of Sensors and Actuators . . . . .	2-15
2.6 Colocation with Lead Compensation . . . . .	2-16
2.7 Non-colocation under Proportional Feedback with Sensor Located at Mass $J_2$ . . . . .	2-17
2.8 Non-colocation under Proportional Feedback with Sensor Located at the Opposite End at Mass $J_3$ . . . . .	2-18
2.9 Non-colocation with a Lead Compensator . . . . .	2-19
3.1 Block Diagram of the Full-state Controller . . . . .	3-4
3.2 Block Diagram of the Kalman Filter . . . . .	3-5
3.3 Block Diagram of the LQG System . . . . .	3-9
3.4 Closed Loop Bandwidths for the Three Element Model . . . . .	3-12
3.5 Root Locus Plot for the LQG Design Without LTR for the Colocated System . . . . .	3-14
3.6 Root Locus Plot for the LQG Design Without LTR for the Non-colocated System . . . . .	3-15
3.7 Loop Transfer Recovery for the Colocated System	3-23
3.8 Root Locus for the LQG Design with LTR for the Colocated System . . . . .	3-23

3.9	LTR for the Non-colocated System . . . . .	3-24
3.10	Root Locus for the LQG Design With LTR for the Non-colocated System . . . . .	3-24
3.11	Step Response Three Element Model . . . . .	3-26
4.1	Free-free Transverse Beam . . . . .	4-2
4.2	Exact Poles/Zeros of a Colocated System . . . . .	4-4
4.3	Exact Poles/Zeros of a Non-colocated System . . . . .	4-4
4.4	Ten Element Transverse Beam . . . . .	4-9
4.5	DOF for the Two Dimensional Element . . . . .	4-9
4.6	Bode Plot Comparing Frequency Response of 11 Modes to the Reduced 4 Modes for the Colocated Beam . . . . .	4-14
4.7	Bode Plot Comparing Frequency Response of 11 Modes to the Reduced 4 Modes for the Non-colocated Beam . . . . .	4-14
4.8	Four Mode Shapes of the Ten Element Beam . . . . .	4-15
4.9	Bode Plots of the Colocated and Non-colocated Ten Element Beam . . . . .	4-18
4.10	Closed Loop Bandwidths for the Ten Element Beam . . . . .	4-20
4.11	Root Locus for the LQG Design Without LTR for the Colocated System . . . . .	4-21
4.12	Root Locus for the LQG Design Without LTR for the Non-colocated System . . . . .	4-22
4.13	LTR for the Colocated System . . . . .	4-23
4.14	Root Locus for the LQG Design with LTR for the Colocated System . . . . .	4-23
4.15	LTR for the Non-Colocated System . . . . .	4-24
4.16	Root Locus for the LQG Design with LTR for the Non-colocated System . . . . .	4-24
4.17	Step Response of the Ten Element Beam . . . . .	4-25

5.1	Contraves P52F Gimbal . . . . .	5-2
5.2	First Mode Showing the Rigid Body Rotation . . .	5-4
5.3	Bode Plots of the Colocated and Non-colocated Contraves Model . . . . .	5-5
5.4	Truncated Model Compared to the Frequency Response for the Colocated Case . . . . .	5-6
5.5	Truncated Model Compared to the Frequency Response for the Non-colocated Case . . . . .	5-6
5.6	8th Order Curve Fit Using Ansys.m to the Frequency Response Data . . . . .	5-7
5.7	Closed Loop Bandwidths for the Contraves Model .	5-9
5.8	LTR for the Colocated Systems . . . . .	5-11
5.9	Root Locus for the LQG Design with LTR for the Colocated System . . . . .	5-11
5.10	LTR for the Non-colocated Systems . . . . .	5-12
5.11	Root Locus for the LQG Design with LTR for the Non-colocated System . . . . .	5-12
5.12	Step Response of the Contraves Gimbals . . . .	5-13

## List of Tables

Tables	Page
2.1 Poles and Zeros of the Transfer Function, Eqn. 2.11 . . . . .	2-12
3.1 LTR for Colocated and Non-colocated Three Element Model . . . . .	3-21
4.1 Eigenvalues from ANSYS and the Closed Form Solution . . . . .	4-10
4.2 Poles and Zeros of the Ten Element Beam . . . . .	4-17
5.1 Poles and Zeros of the Contraves Model . . . . .	5-3
6.1 Comparison of Colocated and Non-colocated Systems	6-4

Abstract

This thesis examines the effects of colocation and non-colocation of sensors and actuators on flexible structures. Colocated structures are easy to stabilize and make robust because they have alternating poles and zeros on the imaginary axis. On the other hand, non-colocated systems are difficult to make robust because they have right half plane (RHP) zeros. Systems with RHP zeros are defined as non-minimum phase systems and have traditionally been avoided in control design.

The thesis uses linear quadratic Gaussian and loop transfer recovery (LQG/LTR) procedures to design optimum controllers for three example problems. The first example studied is a three element single motion degree of freedom (DOF) system analogous to torsional or longitudinal vibration models. Because single motion DOF systems have motion about just one axis, they have no RHP zeros. However, this thesis will show that indeed the non-colocated single motion degree-of-freedom system behaves like non-minimum phase systems.

To model structures with RHP zeros, a finite element model of a Bernoulli-Euler beam is investigated. LQG/LTR controllers are designed for the colocated and non-colocated

systems. Then the closed loop systems are compared for performance and robustness. Finally, a three dimensional finite element model of a Contraves P52F gimbal structure is analyzed. This third example has significantly more complex plant characteristics than the previous two examples. LQG/LTR controllers were designed for this commercially available structure. The results from the different design iterations show that non-colocated structures although they may not be robust can achieve higher performance.

AFIT/GA/ENY/91M-01

EFFECTS OF COLOCATION AND NON-COLOLOCATION  
OF SENSORS AND ACTUATORS  
ON FLEXIBLE STRUCTURES

THESIS

W. C. LEE, Captain, USAF

AFIT/GA/ENY/91M-01

Approved for public release; distribution unlimited.

EFFECTS OF COLOCATION AND NON-COLOLOCATION  
OF SENSORS AND ACTUATORS  
ON FLEXIBLE STRUCTURES

I. INTRODUCTION

Active control systems will be required in the design of Large Flexible Space Structures (LFSS). The future space station is a good example because it will likely consist of a rigid central hub with flexible beam appendages surrounding it. These beams will have many low vibrational modes as a result of maneuvers, motion of mass within the structure and docking procedures [12:521]. Because such low density structures have little damping, the control system must dampen out these vibrational modes. Furthermore, the control system can help increase the size by allowing lighter and more flexible structures to be built. However, the low mass and low frequency modes of such structures can cause problems in keeping it stable.

Not only is the low vibrational modes of the structure a problem, but physical limitations will govern the location of the sensor and the actuator pairs. Ideally, colocated systems are desired because stability is easy to achieve using simple control laws as shown by Gevarter in 1970 [3]. Since that time, most of the control theories and designs have been based

on using colocated systems. But, frequently on space structures, physical limitations prevent colocation. A recent example is the Galileo spacecraft launched by NASA in 1989. It has a separated actuator and sensor pair which made it difficult to control a television camera and other instruments (sensors) located at the end of a flexible beam [4:1]. This beam had four low frequency modes below the required bandwidth. To meet the performance specifications, the controller designed by the Jet Propulsion Laboratory had to be supplemented with a slewing maneuver to minimize vibratory motion. When possible, the sensor and the actuator should be colocated for ease of control design.

In some cases, as stated by Thomas and Schmidt, it is better to have non-colocated sensors and actuators [12:521]. Sometimes the sensor must be placed at a node which gives the most information, but where an actuator can not be placed. A good example (given in Reference 12) is placing a sensor at the tip end of a cantilever beam to measure the largest displacements with its actuator located at the wall. Non-colocated systems also allow greater design flexibility if precise stable control can be exerted at a distance through the flexible structure.

In design of these control systems, whether they are colocated or non-colocated, an accurate mathematical model of the structure is required. When the structure is modeled as a continuous systems, it is described by partial differential

equations. But, for large problems these may be impractical to solve. Instead, computer based Finite Element Method (FEM) is the preferred way to model structures. These models too can become very difficult to solve simply because of its size. Each element has nodes associated with it and each node can have up to six Degrees of Freedom (DOF) for translations and rotations (the DOF represents the unknowns in the problem). Large finite element models are usually truncated to smaller number of modes. But, the truncation introduces more uncertainties and modeling errors to the system. In particular, the truncated models introduce RHP zeros which makes the system non-minimum phase. Traditionally, non-minimum phase systems have been avoided because they are difficult to control. Therefore, the objective of the controller is to make the system robust in the face of uncertainties and model variations.

This thesis examines the effects between colocated and non-colocated sensors and actuators on flexible structures. To truly model the complexities of a flexible system, a commercially available finite element model of a Contraves P52F gimbal structure will be used. First, a simple three element lumped spring-mass system is used to illustrate basic principles of applying control theory to a structure. However, this single motion DOF model does not exhibit any RHP

zeros of a non-minimum phase system usually associated with non-colocation. A two motion degree of freedom system, a transverse beam, is examined to deal with RHP zeros in control design.

The optimal control design techniques of linear quadratic Gaussian and loop transfer recovery (LQG/LTR) are used to control these systems. The design techniques developed for the beam are then applied to the Contraves P52F gimbal. This allows the LQG/LTR design methodology to be used on a structure which exhibits more complex plant characteristics than a transverse beam. Then a thorough design analysis can be evaluated for performance and robustness characteristics between the two types of systems.

The following sections of the thesis first covers the transfer function between the input (actuator) and the output (sensor) for the flexible systems in Chapter II. It will be shown that the poles of the transfer function are the system's natural frequencies; whereas, the zeros are functions of the sensor and the actuator locations. Chapter II also introduces the single motion DOF three element lumped mass model. Chapter III introduces the LQG/LTR theory used to design the controllers for the colocated and the non-colocated systems. The three element model is used to illustrate the concepts of the LQG/LTR theory. Chapter IV presents the transverse beam having RHP zeros for the non-colocated case. Modal equations of motion (EOM) for finite element models is used to derive

the state-space equations which are needed for control theory. Then the LQG/LTR theory is used to design controllers for the finite element transverse beam. Chapter V investigates the gimbal structure which because of its large number of modes is truncated. The control design is compared between the two systems and evaluated for performance and robustness. Finally, Chapter VI summarizes the results and gives recommendations for further study.

## II. BACKGROUND

This section will present a thorough background on the poles and zeros associated with colocated and non-colocated systems. Before analyzing the more complex Contraves P52F gimbal structure, a simpler model will first be examined to illustrate basic principles. A three element model was chosen to simulate the torsional effects of the motor on the gimbal. This model is analogous to studying the longitudinal or the torsional vibration of a system. Because these systems have only motion about one axis, the term single motion DOF will be used in this thesis.

This elementary model can show the effects of colocation and non-colocation of the actuator and the sensor. With colocation it is much simpler to stabilize a system because the transfer function exhibits the desirable property of pole/zero alternation on the imaginary axis. In this case the poles go to the neutrally stable zeros during high gain compensated feedback. Non-colocated systems may have the poles and zeros alternating on the imaginary axis, but they usually have right half plane zeros as well. As discovered by Cannon and Rosenthal [1], non-colocated systems are sensitive to parameter variations and may have "zero flipping".

The three element model for the non-colocated system

examined in this chapter has no zeros. But, it can be shown to behave as a non-minimum phase system. Therefore, one can not necessarily make the assumption that the system is minimum phase because it has no RHP zeros when modeling structures as a single motion DOF system (i.e. longitudinal and torsional vibration models).

## 2.1 POLE/ZERO PATTERNS FOR COLOCATED SYSTEMS

First, the theory on pole/zero alternation is presented below as proved by Martin in Reference 7. Shown below is the transfer function with finite number of modes for a position output sensor,  $y(x,s)$ , and a control force input actuator,  $u(s)$ , for a flexible structure

$$H(s) = \frac{y(x,s)}{u(s)} = \sum_{i=1}^N \frac{h_i g_i}{s^2 + 2\zeta_i \omega_i s + \omega_i^2} \quad (2.1)$$

where  $\omega_i$  = i'th mode natural frequency,  
 $\zeta_i$  = i'th mode damping  
 $s$  is the frequency domain notation after  
 Laplace transformation

The quantities  $g_i$  and  $h_i$  are functions of the location of the sensor and the actuator, respectively, with respect to the

i'th mode shape. The zeros which are a function of  $h_i g_i$  have the following properties as proved by Martin.

Theorem:

A rational function of the form

$$T_N(x) = \frac{N_N(x)}{D_N(x)} = \frac{a_1}{x-b_1} + \frac{a_2}{x-b_2} + \dots + \frac{a_N}{x-b_N} \quad (2.2)$$

with  $a_i \neq 0$ ;  $b_1 > b_2 > \dots > b_N$ ;  $a_i, b_i \in R$ ;

will have alternating poles and zeros on the real axis if, and only if

$$\text{sign}(a_j) = \text{sign}(a_k) \quad \text{for all } j, k.$$

Collorary:

In Eqn 2.2, if

$$\text{sign}(a_i) = \text{sign}(a_{i+1})$$

then  $T_N(x)$  has a real zero between the poles  $b_i$  and  $b_{i+1}$ .

The significance of the alternating poles and zeros as shown by the theorems will be developed in the following sections. The transfer function for a flexible mechanical system given in Eqn 2.1 can be related to that of Eqn 2.2 by

setting  $x = s^2$ ,  $\zeta = 0$ ,  $b_i = -\omega_i^2$ , and  $a_i = h_i g_i$ . Thus an undamped system with poles at

$$s^2 = -\omega_i^2, \quad 1 \leq i \leq N$$

will have zeros at

$$s^2 = -z_k^2, \quad 1 \leq k \leq N$$

with  $w_k^2 < z_k^2 < w_{k+1}^2$ ,

if and only if

$$\text{sign}(h_j g_j) = \text{sign}(h_k g_k) \quad \text{for all } j, k.$$

Eqn 2.1 for the colocated sensor/actuator pair without damping for position output can be expressed as

$$H(s) = \frac{y(0, s)}{u(s)} = \sum_{i=1}^N \frac{a_i}{s^2 + \omega_i^2} \quad (2.3)$$

where  $a_i = h_i g_i$  is the residue of the  $i$ 'th mode shape. Using the mode shape for a longitudinal vibration of a rod as an example (this is also analogous to torsional vibration) [9:158, 15:155], the actuator and the sensor mode shapes are the following:

$$h_i = \sqrt{2}\cos\{i\pi(0)\}, \text{ actuator located at } x = 0,$$

$$g_i = \sqrt{2}\cos\{i\pi(x)\}, \text{ sensor located at distance } x$$

When the sensor and the actuator are colocated at  $x = 0$ , the dot product of  $h_i$  and  $g_i$  becomes  $\sqrt{2}\cos(0)*\sqrt{2}\cos(0) = 2$ . The residues  $a_i$  will always equal 2 and is positive; therefore, the zeros and poles alternate on the imaginary axis as shown in Figure 2.1.

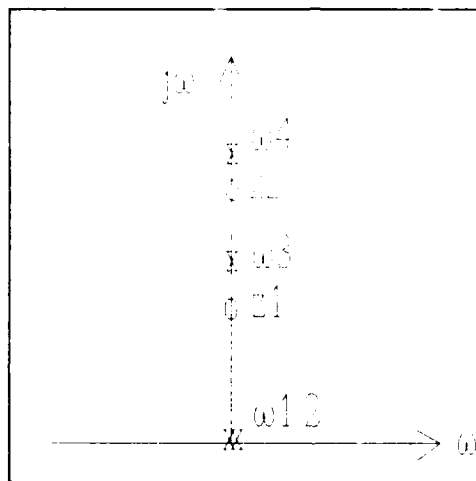


**Figure 2.1** Alternating Poles and Zeros

To stabilize this type of system, the double poles at the origin require a lead compensator to shift them away from the origin. Then the remaining flexible poles will go to the zeros with an angle of departure greater than  $90^\circ$  to remain in the left half plane (LHP). In section 2.3.1, an example of this will be shown.

## 2.2 POLE/ZERO PATTERNS FOR NON-COLOCATED SYSTEMS

Using Eqn 2.3 when the sensor ( $g_i$ ) is located at the opposite end ( $x = 1$ ), the finite transfer function is

$$H(s) = \frac{y(1, s)}{u(s)} = \frac{1}{s^2} + \sum_{i=1}^N \frac{(-1)^i a_i}{s^2 + \omega_i^2} \quad (2.4)$$

$$h_i = \sqrt{2} \cos\{i\pi(0)\} = \sqrt{2}$$

$$g_i = \sqrt{2} \cos\{i\pi(1)\} = +\sqrt{2} \text{ for even number } i \\ = -\sqrt{2} \text{ for odd number } i$$

Clearly, the residues do not have the same sign for all the modes and thus do not have alternating pole/zero pattern on the imaginary axis. Bryson and Wie show that the transfer function Eqn 2.4 for infinite number of modes do not have zeros except at infinity [15:159]. In Reference 15, they derive the product expansion form of Eqn 2.4 from the transcendental transfer functions of a wave equation for single motion DOF systems. Eqn 2.5 shows the zero locations for the three different cases of sensor location used in Section 2.3 for the three element model.

$$H(s) = \frac{y(x, s)}{u(s)} = \frac{1}{s^2} \prod_{k=1}^{\infty} \left( \frac{1 + \frac{s^2}{z_k^2}}{1 + \frac{s^2}{w_k^2}} \right) \quad (2.5)$$

$$\text{where } z_k = \left( \frac{k - \frac{1}{2}}{1 - x} \right) \pi, \quad \omega_k = k\pi$$

For colocation when  $x = 0$ , the zeros,

$$z_k = (k - 1/2)\pi$$

alternates between the poles. For non-colocation when  $x = 1/2$ , the zeros,

$$z_k = (2k - 1)\pi$$

are canceled by the poles. For non-colocation when  $x = 1$ , the zeros,

$$z_k \rightarrow \infty$$

so that  $s^2/\infty = 0$ , and has no zeros.

### 2.3 THREE ELEMENT LUMPED MASS MODEL

This section will examine a single motion DOF system about a single axis for a three element lumped spring-mass model to illustrate the principles used in this thesis. This model is in essence a simple finite element model of a torsional rod. The diagram below shows the lumped spring-mass model and the governing equations of motion.

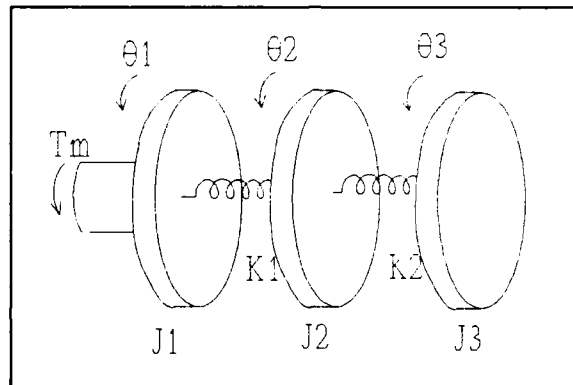


**Figure 2.2** Three Element Lumped Mass Model

$$\begin{aligned} J_1 \ddot{\theta}_1 &= T_m - K_1(\theta_1 - \theta_2) \\ J_2 \ddot{\theta}_2 &= K_1(\theta_1 - \theta_2) - K_2(\theta_2 - \theta_3) \\ J_3 \ddot{\theta}_3 &= K_2(\theta_2 - \theta_3) \end{aligned} \quad (2.6)$$

where

$J_i$  are the moments of inertia,

$\theta_i$  are the angle of rotation,

$T_m$  is the motor torque applied at mass  $J_1$

$K_i$  are the spring constants.

Taking the values for the moments of inertia and the spring constants as unity, the equation simplifies to the following:

$$\begin{aligned}\ddot{\theta}_1 &= -\theta_1 + \theta_2 + T_m \\ \ddot{\theta}_2 &= \theta_1 - 2\theta_2 + \theta_3 \\ \ddot{\theta}_3 &= \theta_2 - \theta_3\end{aligned}\tag{2.7}$$

The output of the measurements of the torsional rotation are the following:

$$\begin{aligned}y_1 &= \theta_1, \\ y_2 &= \theta_2, \\ y_3 &= \theta_3.\end{aligned}$$

These three second order linear equations can be put into the following state space form:

$$\begin{aligned}\dot{x} &= Ax + Bu \\ y &= Cx\end{aligned}\tag{2.8}$$

Defining the following as the state and control vectors

$$x = \begin{pmatrix} \theta_1 \\ \dot{\theta}_1 \\ \theta_2 \\ \dot{\theta}_2 \\ \theta_3 \\ \dot{\theta}_3 \end{pmatrix} \quad u = T_m = \text{input}$$

you have the following state space form for the equations of motion

$$\dot{x} = \begin{bmatrix} 0 & 0 & 0 & 1 & 0 & 0 \\ 0 & 0 & 0 & 0 & 1 & 0 \\ 0 & 0 & 0 & 0 & 0 & 1 \\ -1 & 1 & 0 & 0 & 0 & 0 \\ 1 & -2 & 1 & 0 & 0 & 0 \\ 0 & 1 & -1 & 0 & 0 & 0 \end{bmatrix} \begin{bmatrix} x_1 \\ x_2 \\ x_3 \\ x_4 \\ x_5 \\ x_6 \end{bmatrix} + \begin{bmatrix} 0 \\ 0 \\ 0 \\ 1 \\ 0 \\ 0 \end{bmatrix} u \quad (2.9)$$

$$y = \begin{bmatrix} 1 & 0 & 0 & 0 & 0 & 0 \\ 0 & 1 & 0 & 0 & 0 & 0 \\ 0 & 0 & 1 & 0 & 0 & 0 \end{bmatrix} x$$

Eqn 2.8, the state space equation, can be represented in the frequency domain by the following familiar form of a transfer function.

$$H(s) = C[sI - A]^{-1}B \quad (2.10)$$

For the lumped spring-mass system, the SISO transfer functions are the following:<sup>1</sup>

$$H(s) = \frac{\begin{bmatrix} s^4 + 3s^2 + 1 \\ s^2 + 1 \\ 1 \end{bmatrix}}{s^2(s^4 + 4s^2 + 3)} \quad (2.11)$$

The numerator represents the zeros for the three output locations. Note the first polynomial in the numerator is for the colocated case and the second one is the non-colocated case for  $y_2 = \theta_2$ . The third polynomial which is zeroth order represents the case where the sensor/actuator pair are located on opposite ends. The denominator of the transfer function is the characteristic equation of the model. Solving for the roots of the characteristic equation gives the system poles (structure's natural frequencies). These poles are the same as taking the eigenvalues of the A matrix. The poles and the zeros are listed below in Table 2.1. The table agrees with Eqn 2.5 which shows collocation has alternating zeros and non-collocation does not have zeros.

---

<sup>1</sup>Matlab was used, using `[num,den] = ss2tf(A,B, C, D,1,w)`

**Table 2.1** Poles and Zeros of the Transfer Function, Eqn 2.11

<u>poles</u>	<u>zeros, <math>y_1</math></u>	<u>zeros, <math>y_2</math></u>	<u>zeros, <math>y_3</math></u>
0,0			
$\pm 1.000i$	$\pm .618i$	$\pm 1.000i$	none
$\pm 1.732i$	$\pm 1.618i$		

---

The following are the Bode plots of the magnitude versus frequency for the colocated ( $y_1$  as output) and the non-colocated ( $y_3$  as output) transfer functions. The dips represent the zeros on the imaginary axis and the rises are the poles.

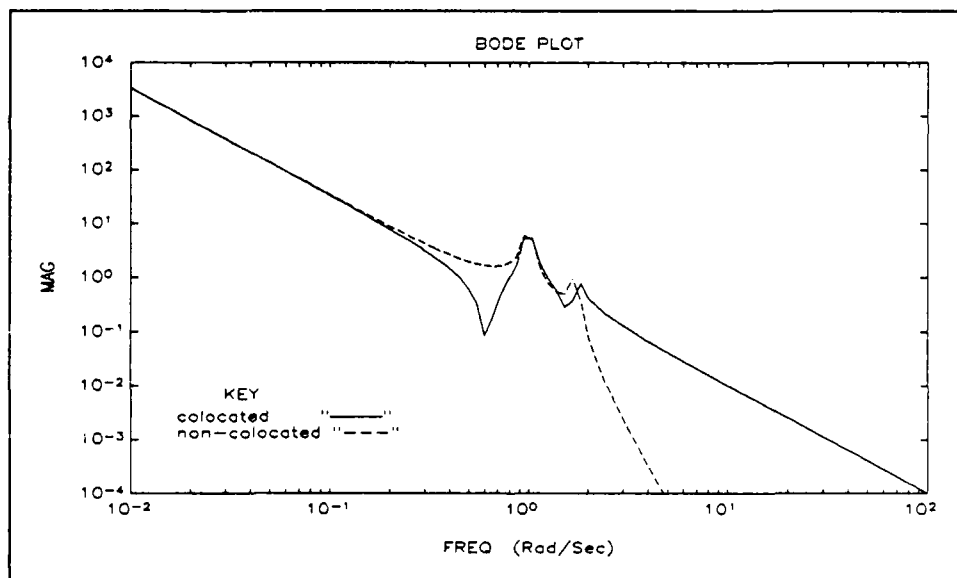


**Figure 2.3** For Colocated,  $y_1$ , and Non-colocated,  $y_3$

### 2.3.1 COLOCATION

The zeros of the transfer function depend on the sensor and the actuator location. One can see from Eqn 2.11 that there are three polynomial equations each representing one of the output cases. For the colocated case ( $y_1 = \theta_1$ ), the second order polynomial,  $s^4 + 3s^2 + 1$ , has zeros (roots of the numerator) as shown in Table 2.1. The poles and zeros are shown to be alternating. Using Eqn 2.2 reveals the transfer function after partial-fraction expansion has all its residues having the same sign. The root locus plot of Figure 2.4 shows the alternating pattern of poles and zeros when the residues have all the same sign as Martin's theorem shows.

To see the robust properties of the colocated system, the root locus for open loop plant for the system in Figure 2.4 will be plotted.

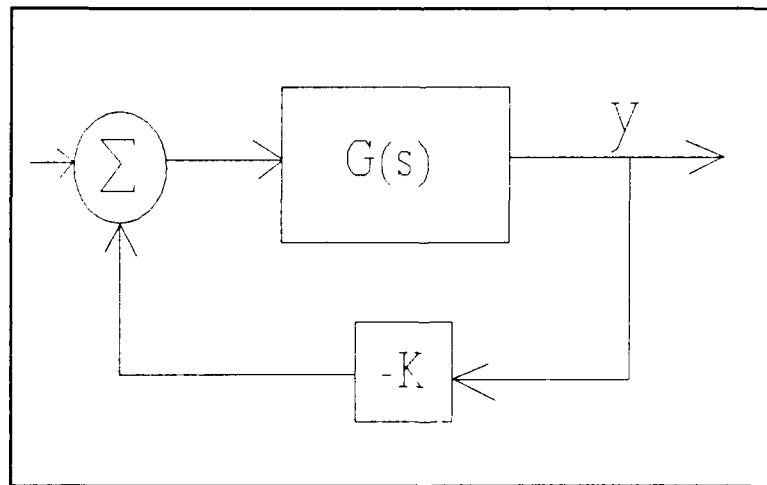


**Figure 2.4** Closed Loop System with Unity Feedback and Proportional Gain

The following equation represents the closed loop transfer function of the plant under unity feedback with proportional gain.

$$G_{cl}(s) = \frac{kG(s)}{1 + kG(s)} \quad (2.12)$$

where  $G(s)$  represents the transfer function of the open loop plant.

$k$  = proportional feedback of the output with no compensation

The root locus plot of Figure 2.5 contains the poles of the solution to the characteristic equation of Eqn 2.12 as gain  $k$  increases. The plot reveals one of the rigid body poles (there are two at the origin) are destabilized immediately while the flexible poles are marginally stable on the imaginary axis.

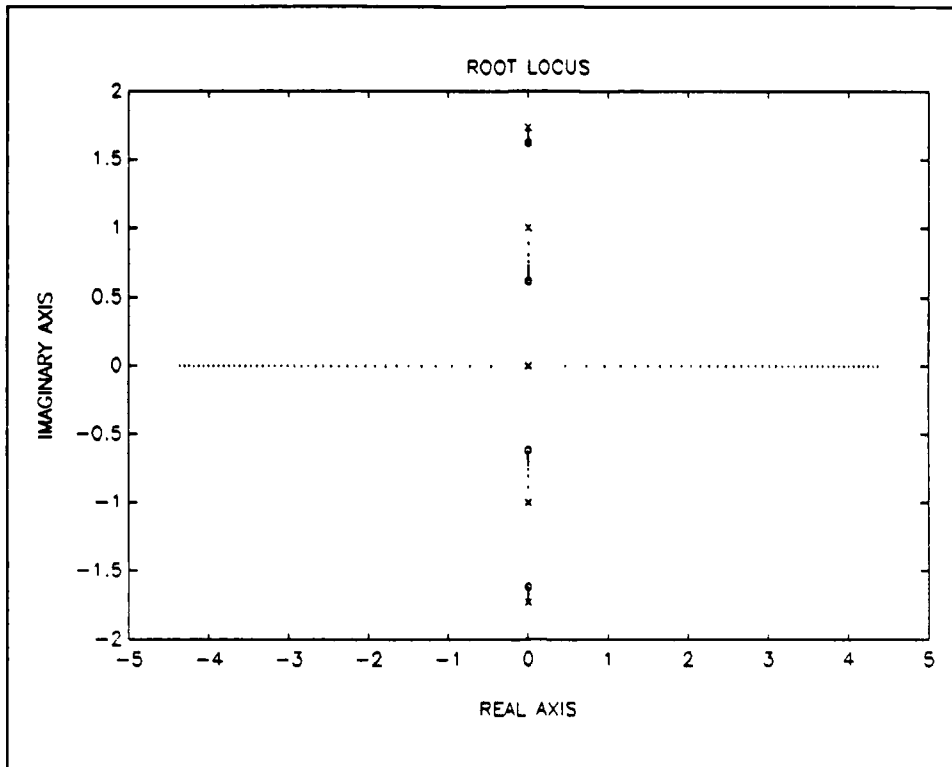


**Figure 2.5** Colocation of Sensors and Actuators

The system is clearly unstable for proportional compensation. But, a simple lead compensator can stabilize the plant as shown in Figure 2.6.

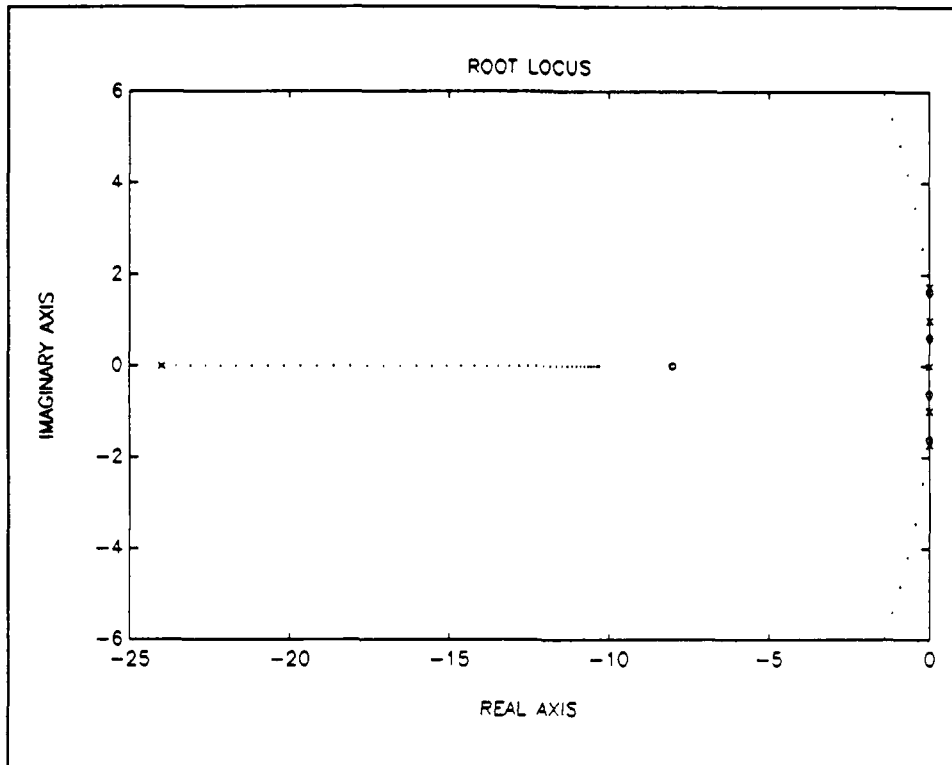


**Figure 2.6** Colocation with Lead Compensation

The compensator used is the following:

$$G_{CL} = -32 \left( \frac{s + 8}{s + 24} \right) \quad (2.11)$$

As depicted in Figure 2.6, the colocated system remains stable even under high gain feedback. The gain value was increased from .5 to 20.

### 2.3.2 NON-COLOCATION

For the case where the sensor is located in the middle ( $y_2 = \theta_2$ ), there is an excess pole which causes the root locus plot to go unstable during proportional feedback as shown in Figure 2.7.

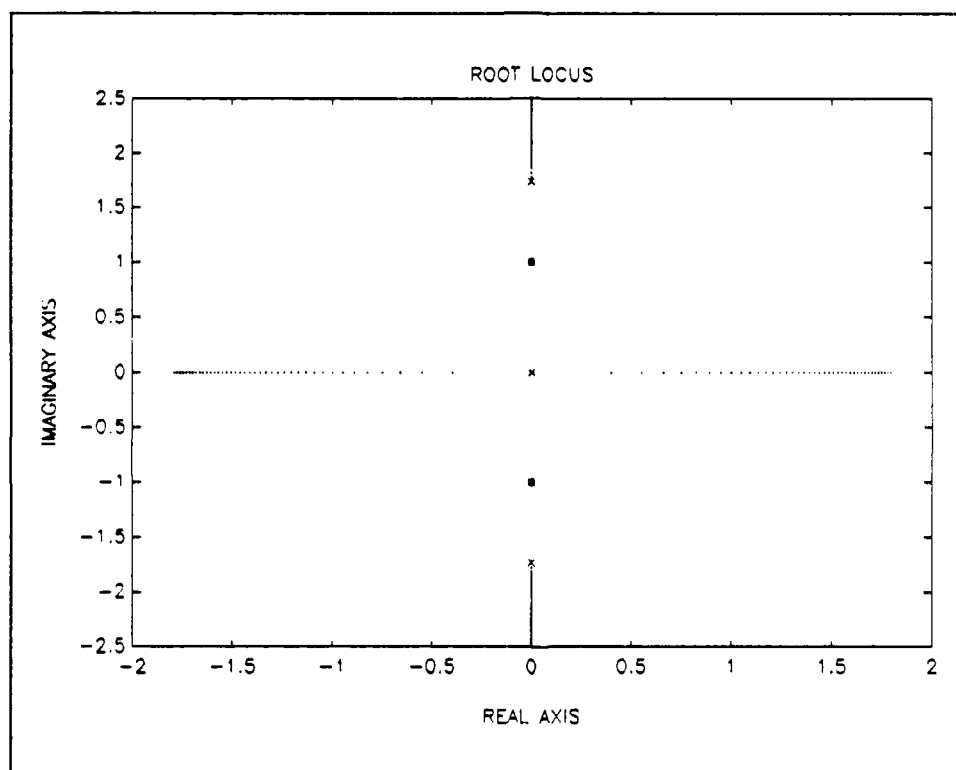


**Figure 2.7** Non-colocation Under Proportional Feedback with the Sensor Located at Mass  $J_2$

Partial-fraction expansion reveals this non-located system does not all have the same sign for its residues, so, the system does not have alternating poles and zeros. This is clear by examining the poles and zeros in Table 2.1. In fact,

this system has the undesirable property of being unobservable because the zeros cancel one of the poles. For the third case where the sensor and the actuator are located on opposite ends of the structure, there are no zeros. Therefore the system is clearly unstable during proportional feedback as shown in Figure 2.7.

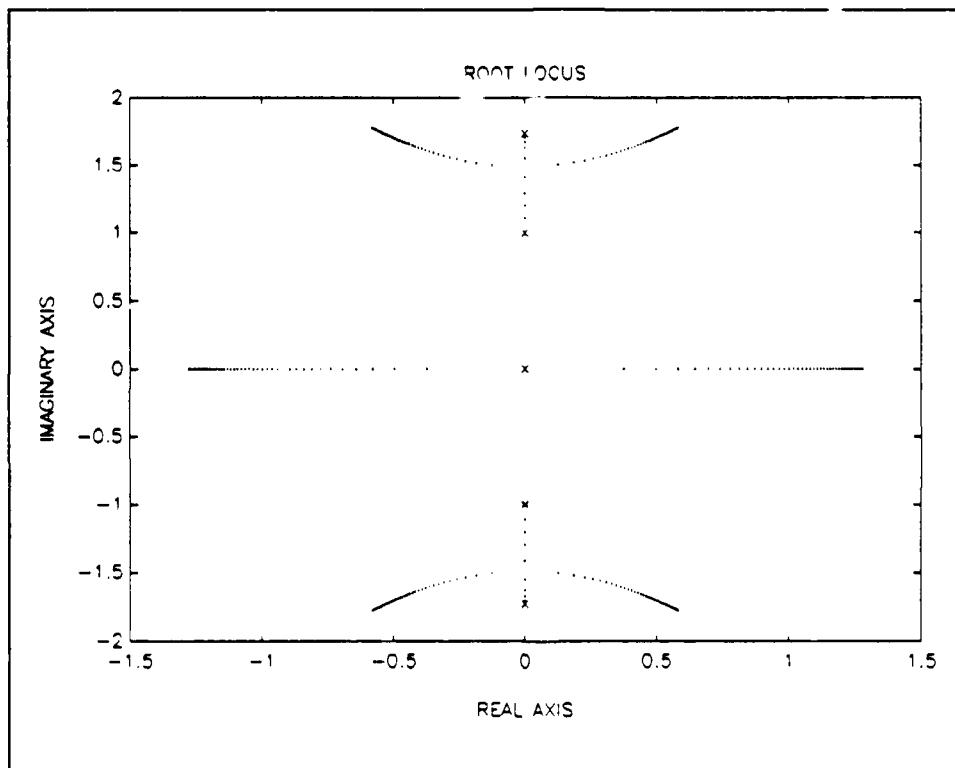


**Figure 2.8** Non-collocated Case Under Proportional Feedback with Sensor at the Opposite End at Mass  $J_3$

Using a simple lead compensator as in the collocated case, the first flexible pole is immediately destabilized as shown in the root locus plot in Figure 2.8. The transfer function for the lead compensator used is

$$G_{CL} = -.3 \left( \frac{s + .2}{s + .6} \right)$$

In the non-colocated case, a lead compensator is ineffective. To achieve stability, a higher order compensator is clearly needed. For this thesis, the Linear Quadratic Gaussian (LQG) design techniques will be used to design the controller.

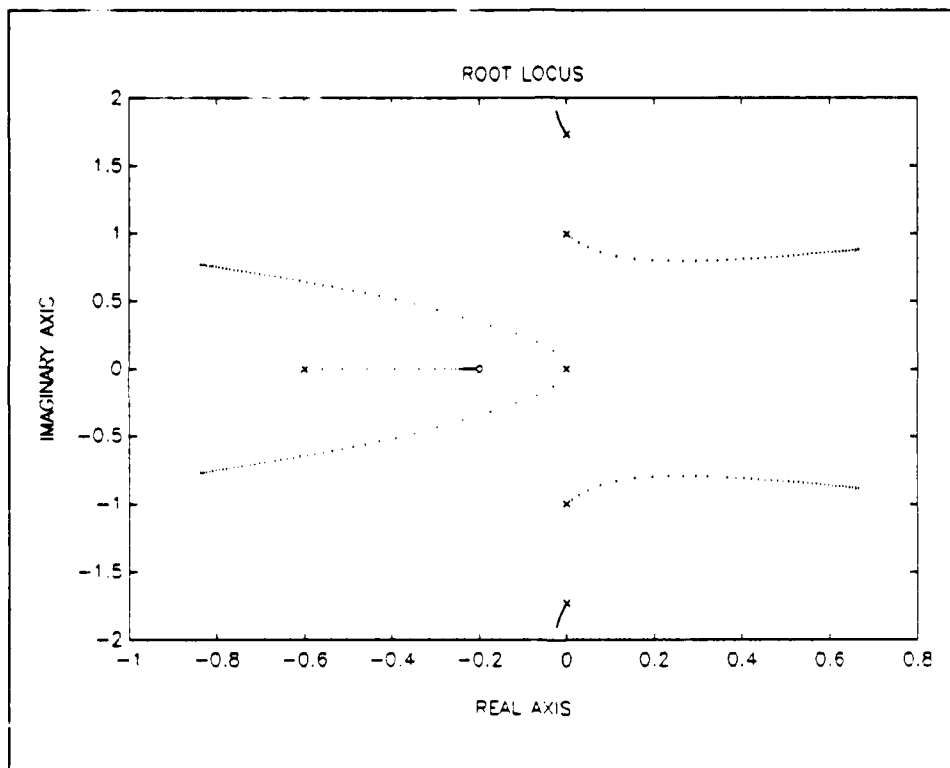


**Figure 2.9** Non-colocation With a Lead Compensator

### III. LINEAR QUADRATIC GAUSSIAN / LOOP TRANSFER RECOVERY

#### 3.1 LQG/LTR THEORY

Linear Quadratic Gaussian/Loop Transfer Recovery (LQG/LTR) theory is used to design the controllers to increase the performance and robustness of the control systems presented in this thesis. The first step to the LQG/LTR method is to design the Linear Quadratic Gaussian (LQG) controller. A quadratic performance index is used to define the LQG controller; therefore, it produces an optimal control design stabilizes the closed loop system for the given design conditions. The LQG controller is comprised of the Linear Quadratic Regulator (LQR) and the Linear Quadratic Estimator (LQE). The LQR is a full-state feedback controller and the LQE is an estimator, commonly called the Kalman filter.

The LQG/LTR design method modifies the standard LQE and recovers the guaranteed robustness of the full-state regulator. This results in a closed loop system (the combined plant and the compensator) that is robust to uncertainties, disturbances and gain increases. The LQG/LTR methodology is also ideal for multi-input-multi-output (MIMO) systems. The following section will first introduce the basics of the full-state feedback control theory. Then, the estimator and the

LQG controller will be presented. Finally, loop transfer recovery is developed. These sections briefly introduce the optimal control theory which is presented in more detail in many other references. In particular the technical report, Introduction to Robust Multivariable Control, by Ridgely and Banda is extensively used by the author to develop the next four sections [10].

### 3.2 LINEAR QUADRATIC REGULATOR

The linear quadratic regulator as taken from chapter 6 of Ridgely and Banda is the following. The LQR relies on minimizing the quadratic performance index

$$J = \int_0^{\infty} [x^T(t) Q_c x(t) + u^T(t) R_c u(t)] dt \quad (3.1)$$

for the state-space Eqn 2.9.

The weighting matrices  $Q_c$  and  $R_c$  are chosen by the designer depending on the importance of the state or the control vectors. If the  $[A, B]$  pair is stabilizable, then the optimal control law is

$$u = -K_c x \quad (3.2)$$

The gain matrix,  $K_c$ , is given by

$$K_c = R_c^{-1} B^T P \quad (3.3)$$

where  $P$  is the symmetric positive semi-definite matrix solution to the algebraic Riccati equation

$$0 = A^T P + P A - P B R_c^{-1} B^T P + Q_c \quad (3.4)$$

where selecting  $Q_c = Q_c^T \geq 0$  (positive semi-definite) is a sufficient condition for asymptotic stability of the closed-loop system.  $R_c$  must be positive definite. Substituting the control law, Eqn 3.2, into Eqn 2.9 yields the closed loop system.

$$\begin{aligned} \dot{x} &= A x + B [-K_c x] \\ &= [A - B K_c] x \end{aligned} \quad (3.5)$$

Figure 3.1 depicts the state space system of Eqn 3.5.

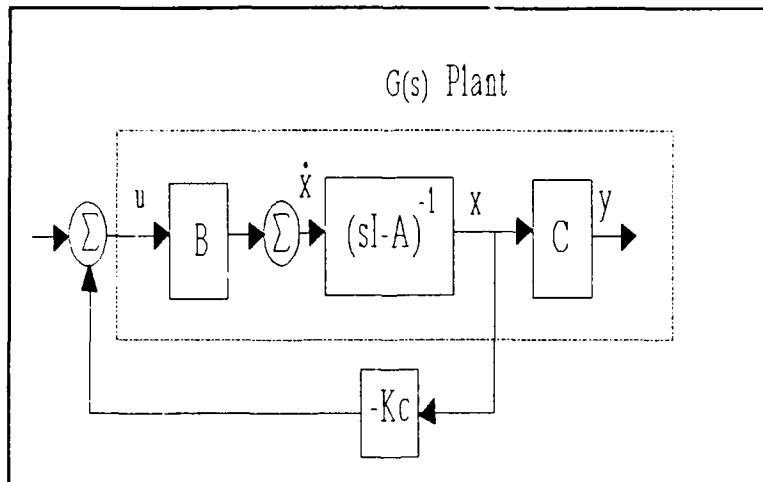


**Figure 3.1** Block Diagram of the Full-state Controller

### 3.3 LINEAR QUADRATIC ESTIMATOR

The one drawback of using the full-state regulator is it assumes all the states can be measured. It is frequently impossible or very expensive to measure all the states (many sensors may be required on a space structure); therefore, an estimator must be used to model the system. This estimator must also take into account disturbances in the system. The familiar state-space equation now including disturbances is

$$\dot{x} = Ax + Bu + \Gamma w \quad (3.6)$$

$$y = Cx + v \quad (3.7)$$

where  $w$  and  $v$  are input and output disturbances, respectively.

The disturbances are assumed zero-mean Gaussian stochastic processes which are uncorrelated in time and have the covariances

$$E[ w(t)w^T(\tau) ] = Q_0\delta(t-\tau) \geq 0,$$

$$E[ v(t)v^T(\tau) ] = R_f\delta(t-\tau) > 0$$

The covariance matrix  $Q_0$  is positive semi-definite;whereas,  $R_f$  is positive definite. The correlation between  $w$  and  $v$  will be assumed to be zero

$$E[ w(t)v^T(t) ] = 0$$

Equation 3.6 and the Kalman filter are represented by the block diagram below.

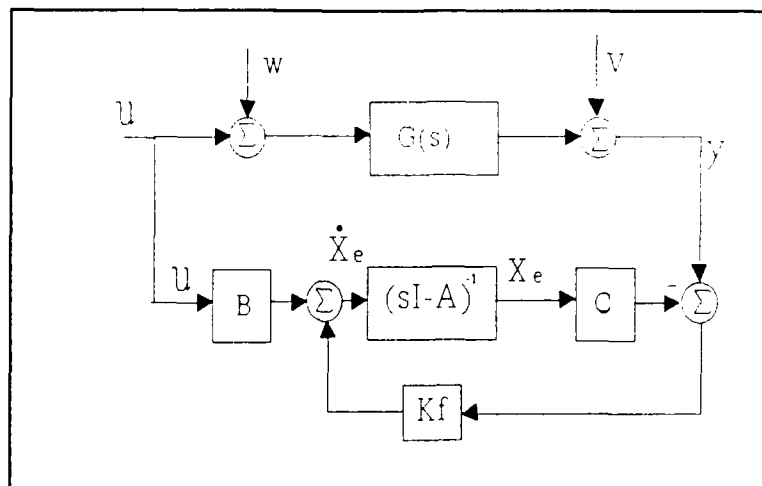


**Figure 3.2** Block Diagram of the Kalman Filter

The equation for the estimator is given by

$$\dot{\hat{x}}_e = A\hat{x}_e + Bu + K_f(Y - C\hat{x}_e) \quad (3.8)$$

where  $\hat{x}_e$  is the estimate of the states.

The following development of the Kalman filter is taken directly from Ridgely and Banda. First, an assumption must be made: the input and output disturbances,  $w$  and  $v$ , are time-invariant and wide-sense stationary. Then the matrices  $Q_0$  and  $R_f$  are constant. This is a valid assumption as long as the observation of the output is much greater than the dominant time constants of the system. The Kalman filter gain matrix,  $K_f$ , minimizing the mean-square error

$$E[e^T e] \quad (3.9)$$

where

$$e = x - \hat{x}_e \quad (3.10)$$

is

$$K_f = \Sigma C^T R_f^{-1} \quad (3.11)$$

$\Sigma$ , the variance of the error function, is found by solving the algebraic variance Riccati equation

$$0 = A\Sigma + \Sigma A^T - \Sigma C^T R_f^{-1} C \Sigma + Q_f \quad (3.12)$$

with  $Q_f = \Gamma Q_0 \Gamma^T$ . Frequently,  $\Gamma = I$  (meaning each state has its own distinct process noise).

The algebraic variance Riccati equation shown in Eqn 3.12 has several solutions, for which the correct solution is unique and positive definite. A sufficient condition for  $\Sigma$  to exist is that the pair  $[A, C]$  be completely observable. This condition may be relaxed to detectability, in which case it is necessary and sufficient and  $\Sigma$  may be positive semidefinite. Given that  $\Sigma$  exists, the error dynamics of the filter are

$$\begin{aligned}\dot{e} &= \dot{x} - \dot{x}_e & (3.13) \\ &= [Ax + Bu + \Gamma w] - [Ax_e + Bu + K_f\{y - Cx_e\}] \\ &= [A - K_f C]e + [\Gamma - K_f][w \ v]^T\end{aligned}$$

Therefore, the poles of  $[A - K_f C]$  are the poles of the estimator error response. The poles must be asymptotically stable (the error must be getting smaller) if and only if the pair  $[A, \Gamma]$  is stabilizable.

### 3.4 LINEAR QUADRATIC GAUSSIAN

Combining the results of LQR and LQE gives the following expression for the LQG compensator

$$\begin{aligned}\dot{x}_e(t) &= Ax(t) - BK_c x_e(t) + K_f[y(t) - Cx_e(t)] \\ &= (A - BK_c + K_f C)x_e(t) + K_f y(t)\end{aligned}\quad (3.14)$$

Taking the Laplace transform yields the following

$$x_e(s) = [sI - A + BK_c + K_f C]^{-1} K_f y(s) \quad (3.15)$$

Now, substituting this into the control law (dropping the s notation)

$$u = -K_c x_e \quad (3.16)$$

yields the expression for the LQG compensator

$$u = -K_c [sI - A + BK_c + K_f C]^{-1} K_f y \quad (3.17)$$

substituting the plant transfer function without the noises, w and v,

$$y = C(sI - A)^{-1} Bu \quad (3.18)$$

gives

$$u = -K_c [sI - A + BK_c + K_f C]^{-1} K_f C(sI - A)^{-1} Bu \quad (3.19)$$

The following figure represents the Eqn 3.19 for the LQG compensator and the plant.

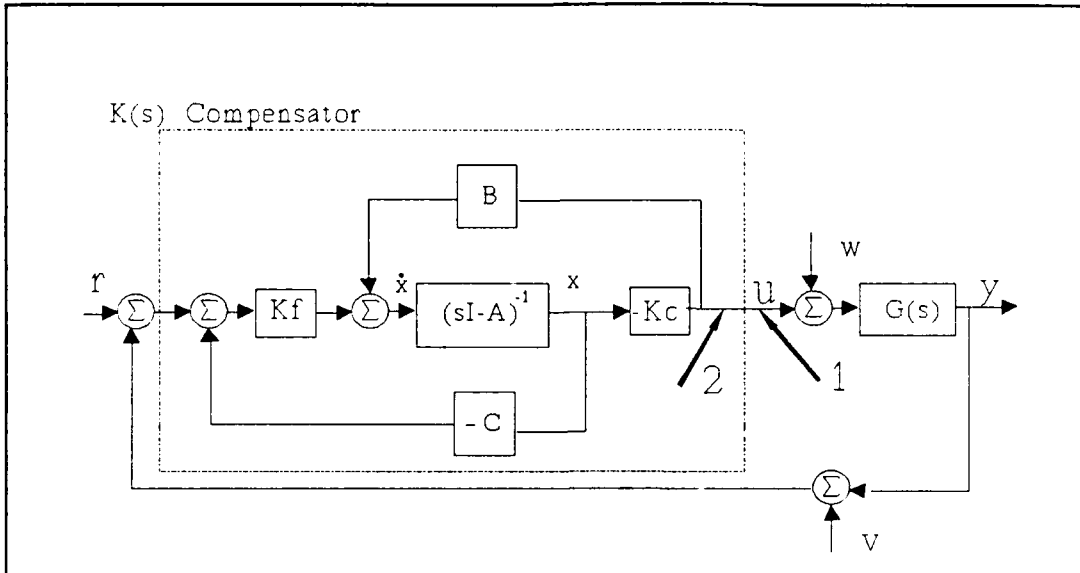


**Figure 3.3.** Block diagram of the LQG system.

The poles of the LQG compensator are seen to be solutions of

$$\det[sI - A + BK_c + K_f C] = 0$$

Although the poles of the regulator, the estimator and the closed loop system are all stable, the LQG compensator poles are not always stable. The eigenvalues of the closed-loop system are evaluated to prove the stability. Taking the two equations we have for the state

$$\dot{x} = Ax + B[-K_c x_e] + \Gamma w \quad (3.20a)$$

$$\dot{x}_e = (A - BK_c + K_f C)x_e + K_f Cx + K_f v \quad (3.20b)$$

Remembering that

$$\dot{e} = \dot{x} - \dot{x}_e \quad (3.13)$$

We can put Eqn 3.20a and Eqn 3.20b into its state space form

$$\begin{bmatrix} \dot{x} \\ \dot{e} \end{bmatrix} = \begin{bmatrix} A - BK_c & BK_c \\ 0 & A - BK_f C \end{bmatrix} \begin{bmatrix} x \\ e \end{bmatrix} + \begin{bmatrix} \Gamma & 0 \\ \Gamma & -K_f \end{bmatrix} \begin{bmatrix} w \\ v \end{bmatrix} \quad (3.21)$$

Using Schur's formula, the above equation can be broken into its determinant form

$$\det[sI - A + BK_c] \cdot \det[sI - A + K_f C] = 0 \quad (3.22)$$

Eqn 3.22 shows that the LQG compensator is composed of the regulator and the estimator poles which are stable. Therefore, the closed loop LQG systems are always stable, although the compensator itself may not be stable. An example of this unstable compensator will be shown in the next section.

### 3.5 LQG DESIGN ON THREE ELEMENT MODEL

The Linear Quadratic Gaussian (LQG) design technique developed in section 3.4 will be used to develop a sixth order

compensator (same order as the plant) for both the colocated and non-colocated cases. To make a fair design comparison, the closed loop bandwidths for the two systems were made equal. This bandwidth was pushed as close as possible to the lowest frequency zero. This ensures the flexible poles will have an effect the plant and the controller.

Briefly, the LQ Regulator is designed for the highest bandwidth it can achieve by varying the state space weighting matrix,  $Q_c$ . The bandwidth achievable is limited by the first imaginary zero which causes the closed loop gain to go below the -3 dB line quickly. Then, the LQ Estimator is calculated by estimating the noise matrices,  $Q_o$  and  $R_f$ . This thesis uses an approximate noise intensity for  $Q_o$  as ten percent of the input force. The regulator and the estimator are then combined to construct the LQG controller. In each case, the design is iterated by varying the  $Q_c$  weighting matrix for the LQR until they have approximately the same bandwidth. See Figure 3.4.

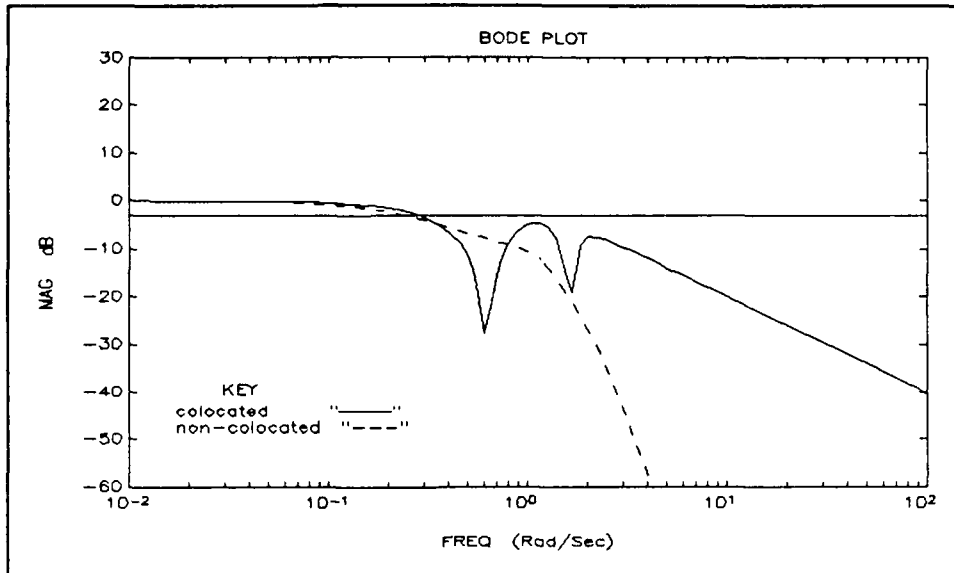


**Figure 3.4** Closed Loop Bandwidths for the Three Element Model

The procedure leading to the LQG design was facilitated by using a MATLAB script file, LQGD.M (See Appendix C for the program). The weighting matrices used for the LQR for the colocated case is

$$Q_c = \text{diag}(10 \ 10 \ 10^5 \ 10^5 \ 10^5 \ 10^5),$$

and for the non-colocated case is

$$Q_c = \text{diag}(10 \ 10 \ 10 \ 10 \ 10^{2.5} \ 10^{2.5}).$$

For both cases, the noise intensity at the input for the LQE is chosen as

$$Q_o = 10^2.$$

After designing the LQG controller the root locus of the closed-loop system is plotted to check the stability robustness. The transfer function of the LQG controller for the colocated case is

$$K_{LQG} = \frac{(s + .177) (s + .19 \pm .892i) (s + .37 \pm 1.637i)}{(s + 316.2) (s + 3.125) (s + .155 \pm .838i) (s + .35 \pm 1.62i)}$$

Figure 3.5 shows the root locus plot of the closed loop colocated system. The compensated plant remains stable for all gains in the range 0.5 to 30.0.

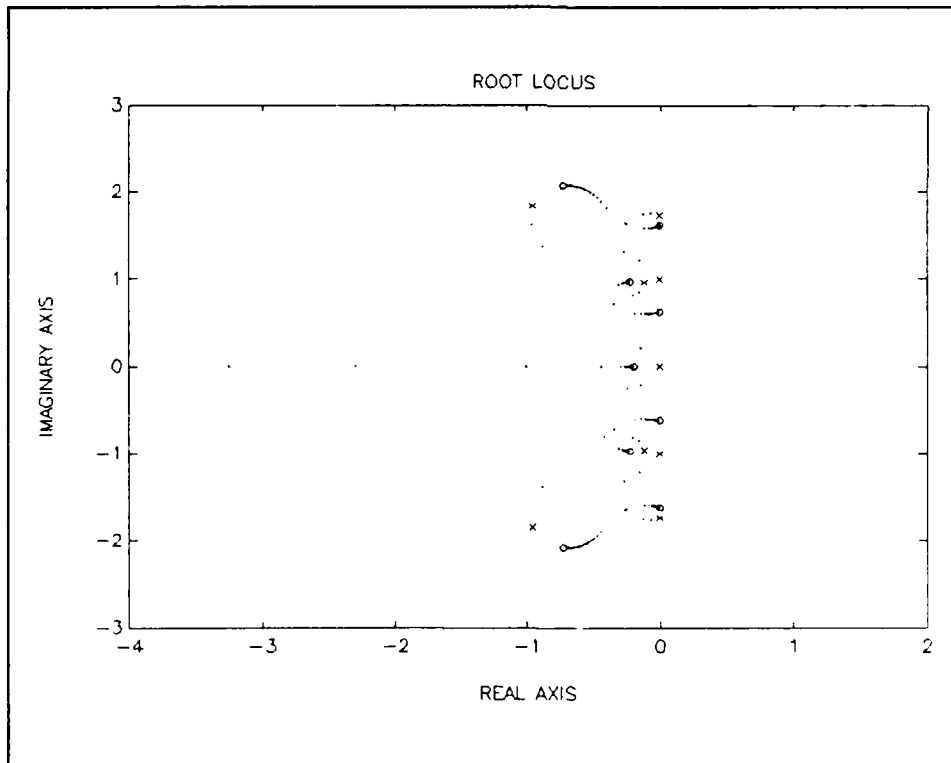


**Figure 3.5** Root Locus for the LQG Design without LTR for the Colocated System

The transfer function of the LQG controller for the non-colocated case is

$$K_{\text{LQG}} = \frac{(s + .12) (s + 1.72) (s - 7.5) (s + .208 \pm 1.07i)}{(s + 1.304) (s + 3.1) (s + 1.33 \pm 1.56i) (s + .952 \pm 2.11i)}$$

Figure 3.6 shows the root locus of the non-colocated closed loop system. With increasing gain, the closed loop poles of the compensator and the plant move into the right half plane after a gain of  $k=1.75$ . This is a seventy-five percent gain increase from the nominal design, but it is not as robust as the colocated system which remains stable for gains up to  $k = 30$ . One can see that LQG does not guarantee stability in the face of uncertainties. In fact, for the non-colocated system, it goes unstable rather easily. In other words, the controller is not robust and LTR techniques are needed.

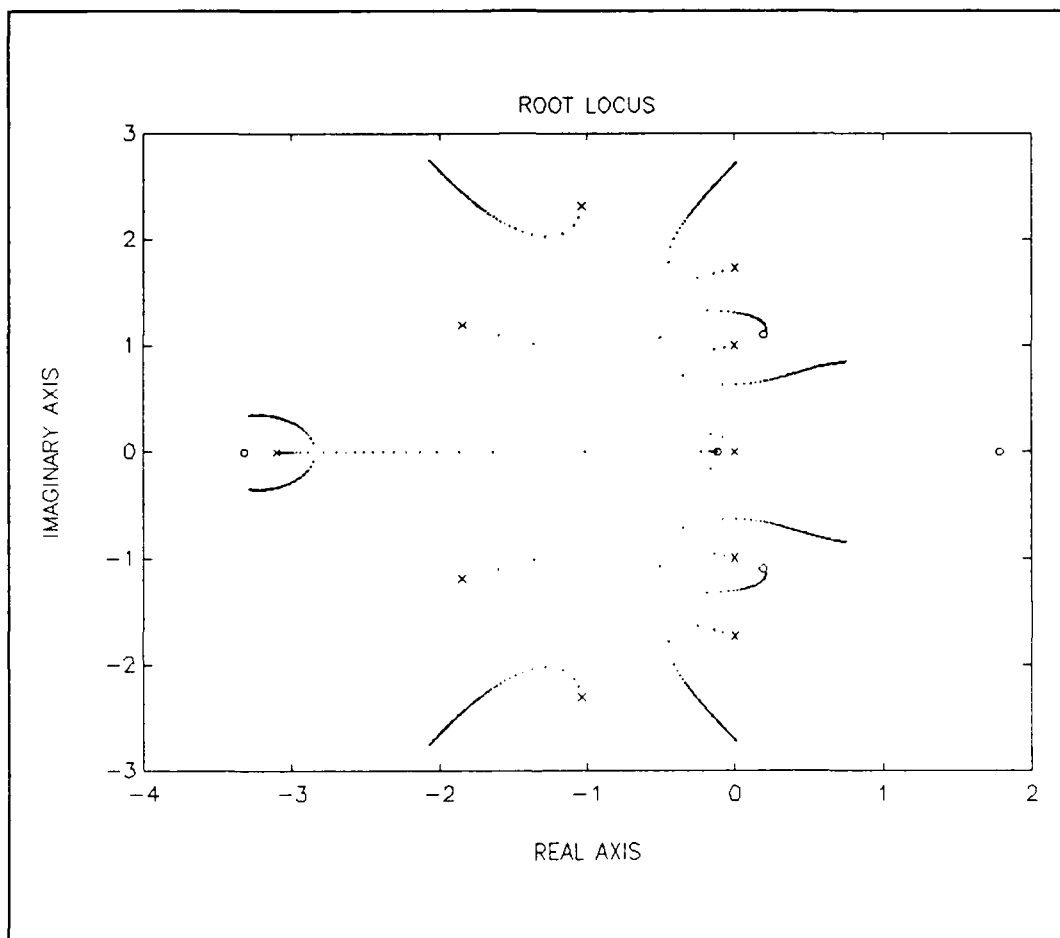


**Figure 3.6** Root Locus for the LQG Design without LTR for the Non-colocated System

### 3.6 LOOP TRANSFER RECOVERY

As mentioned in section 3.5, the disadvantage of the LQG compensator is that it is generally not robust. The three element non-colocated example went unstable after a small gain increase. One reason is that the estimator inserted into the LQG loop no longer guarantees the stability margins from the full-state feedback regulator. Loop recovery technique must be used by adjusting the Kalman filter gains.

In looking at Figure 3.3 of the LQG block diagram, the return ratio (the characteristic equation of the SISO transfer function) at point marked 1 determines the robustness and performance properties for the plant,  $G(s)$ . The return ratio at point 1 is

$$K(s)G(s) = -K_c[sI - A + BK_c + K_f C]^{-1} K_f C (sI - A)^{-1} B \quad (3.23)$$

If you break the loop at point 1, the return ratio at point 2 is the full state feedback controller

$$K_{LQR}(s) = K_c (sI - A)^{-1} B \quad (3.24)$$

The reason is when you break the loop at point 1, the signal to the Kalman filter matrix  $K_f$  is zero. This assumes that the  $A$ ,  $B$ , and  $C$  matrices of the filter match those of the plant exactly. Thus, the gist of the LTR theory is to make the

return ratios at points 1 and 2 to be the same. The following is taken from Maciejowski [6:232].

Let  $\Phi = (sI - A)$  and rewrite Eqn 3.23 without the frequency domain notation ( $s$ ) for brevity.

$$K(s)G(s) = -K_c[\Phi + BK_c + K_f C]^{-1}K_f C \Phi^{-1}B \quad (3.25)$$

Without going into the formal proof which is shown in Ridgely and Banda [10:ch. 8] and Maciejowski [6:232-234], one can see how Eqn 3.25 becomes 3.24 by observing what happens as  $K_f$  is increased toward infinity. At low frequencies ( $s = j\omega$ ), the term inside the bracket,  $\Phi + BK_c$ , becomes much smaller than  $K_f C$ . Thus, the bracketed term approaches  $[K_f C]^{-1}$ . This leads to

$$K(s)G(s) = -K_c [K_f C]^{-1} K_f C \Phi^{-1}B \quad (3.26)$$

$$K(s)G(s) = -K_c I \Phi^{-1}B$$

$$K(s)G(s) = -K_c \Phi^{-1}B$$

Intuitively, Eqn 3.26 shows that at low frequencies and high estimator gains the LQG controller and the plant approaches the behavior of a full state regulator. In terms of poles and zeros, the effect of increasing the gain  $K_f$  causes the closed loop poles of the Kalman filter to notch out the plant zeros. The plant poles then move toward the

compensator zeros. In turn, these compensator zeros approach the closed loop pole locations of the full-state regulator and thus achieves the robustness guaranteed by the LQR. One can then increase the robustness over large a bandwidth by increasing the gain  $K_f$ . See the LTR plots of Figure 3.7 and Figure 3.9 in Section 3.7 for examples.

However, there is a design trade off because increasing the filter gains also increases the system noise response. One thing to keep in mind is that increasing the gain no longer makes it a true Kalman filter. The noise intensity is changing from the initial assumed  $Q_f = Q_0$ . See the equation below when the loop transfer recovery is applied at the plant input.

$$Q_f = Q_0 + q^2 BVB^T$$

$$R_f = R_0$$

$V$  is any postive definite symmetric matrix and is usually taken as identity.  $Q_0$  and  $R_0$  are the actual noise intensities. The second term with  $q^2$  is the additional fictitious output noise associated with LTR. When  $q = 0$ , it becomes the standard Kalman filter.

### 3.6.1 ROOT MEAN SQUARE RESPONSE

The effect of the increasing the fictitious noise on the system can be measured by the Root Mean Square (RMS) response for the LQG/LTR closed loop system. The covariance of the output must be found by first solving the Lyapunov equation for the state variance [5:104].

$$AQ_x + Q_x A^T + BVB^T = 0 \quad (3.27)$$

where

$$Q_x = E(xx^T)$$

$$V = I$$

A and B are from state space equation

The output covariance is then

$$Q_y = E(yy^T)$$

which after combining with Eqn 3.27 becomes

$$Q_y = CQ_x C^T \quad (3.28)$$

The RMS response is found by simply taking the square root of the diagonal of the covariance in Eqn 3.28.

### 3.6.2 LTR WITH NON-MINIMUM PHASE SYSTEMS

LTR theory is not guaranteed to work with non-minimum phase systems. Maciejowski states that some of the Kalman filter's eigenvalues or poles from the LQG design moves toward the plant's zeros [6:231]. This implies LTR can only be used for minimum phase plants since the eigenvalues of the closed-loop regulator and the estimator cannot be in the left half plane. However, LTR may still work if the right half plane zeros are above the cross-over frequency.

### 3.7 LOOP TRANSFER RECOVERY ON THE THREE ELEMENT MODEL

For the three element model, the colocated system shows excellent loop recovery properties throughout its frequency range ( $10^{-2}$  to  $10^2$  rad/sec). Examination of the system eigenvalues shows that the poles of the plant and the compensator moving toward the poles of the full-state controller. Figure 3.7 shows clearly the open loop system approaching the target loop of the full-state. The high fictitious noise of  $10^{15}$  was able to get full recovery (as evident by the loop matching the full state). The root locus of the closed loop  $K(s)G(s)$  system shows it retains excellent robustness with the poles going unstable after a gain increase of  $k = 28.5$  at  $q^2 = 10^{15}$ . This is almost a three-thousand

percent gain variation that the colocated system can handle! See Figure 3.8 for the root locus plot.

The non-colocated system does improve its robustness slightly with LTR, although loop recovery is not as easy to achieve with the non-colocated system (indication that this type of system is non minimum phase). See Figure 3.9 for  $q^2 = [ 0 \ 10^{18} \ 10^{20} ]$ . Notice the good recovery at low frequencies, but not at high frequencies. In fact there are small spikes in the loops where it diverges from the full state's open loop. Using a large fictitious noise value of  $10^{20}$  did get good recovery and damped out the spike. It also improved the robustness of the system to gain variations up to  $k = 4$ . See Table 3.1

**Table 3.1** LTR for Colocated and Non-colocated Three Element Model

<u><math>q^2</math></u>	<u>colocated</u>	<u>non-colocated</u>
0	30	1.75
$10^3$	30	1.75
$10^6$	17.0	1.25
$10^9$	6.5	1.50
$10^{12}$	8.0	1.50
$10^{15}$	28.5	2.0
$10^{18}$	30	2.75
$10^{20}$	30	4.0
$10^{24}$	30	7.0

The table shows a decrease in the colocated system when  $q^2 = 10^9$  and  $10^{12}$ . Starting at these fictitious noise values,

the colocated RMS response becomes greater. Then the RMS response stabilizes after  $q^2 = 10^{15}$ . See Table A.1 in Appendix A. Thus, the increase in the noise of the colocated system appears to have an effect on the robustness of the system to loop transfer recovery.

In looking at the LTR plots and the Bode plots, the non-colocated system has the advantage of having the high frequency roll-off. This is desirable to prevent the noise from amplifying and driving the system unstable. The non-colocated system does have a major drawback in that it behaves like a non-minimum phase system with RHP zeros. Figure 3.10 shows the root locus plot using the fictitious noise value of  $10^{18}$ . Note the poles moving into the right half plane as if there were RHP transmission zeros.

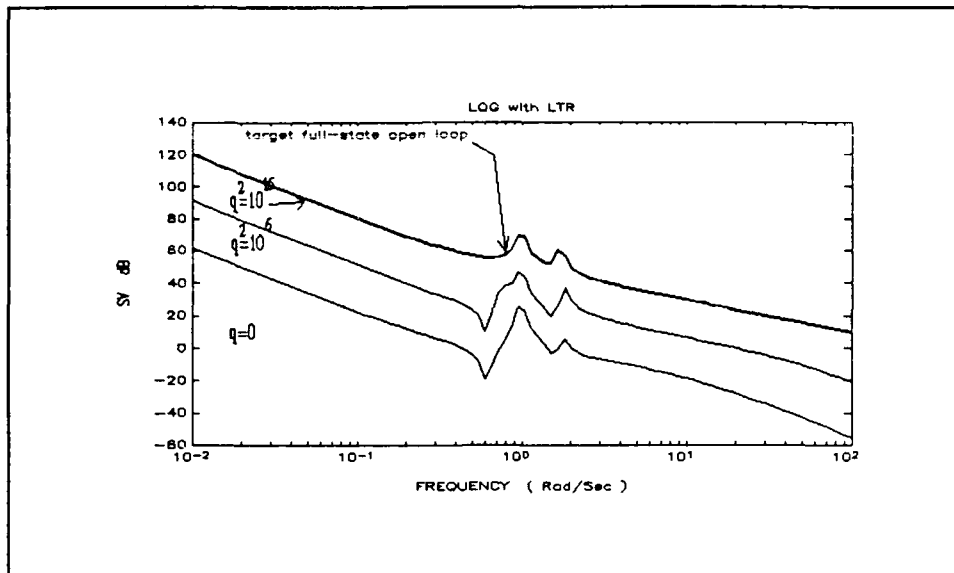


**Figure 3.7** LTR for the Colocated System

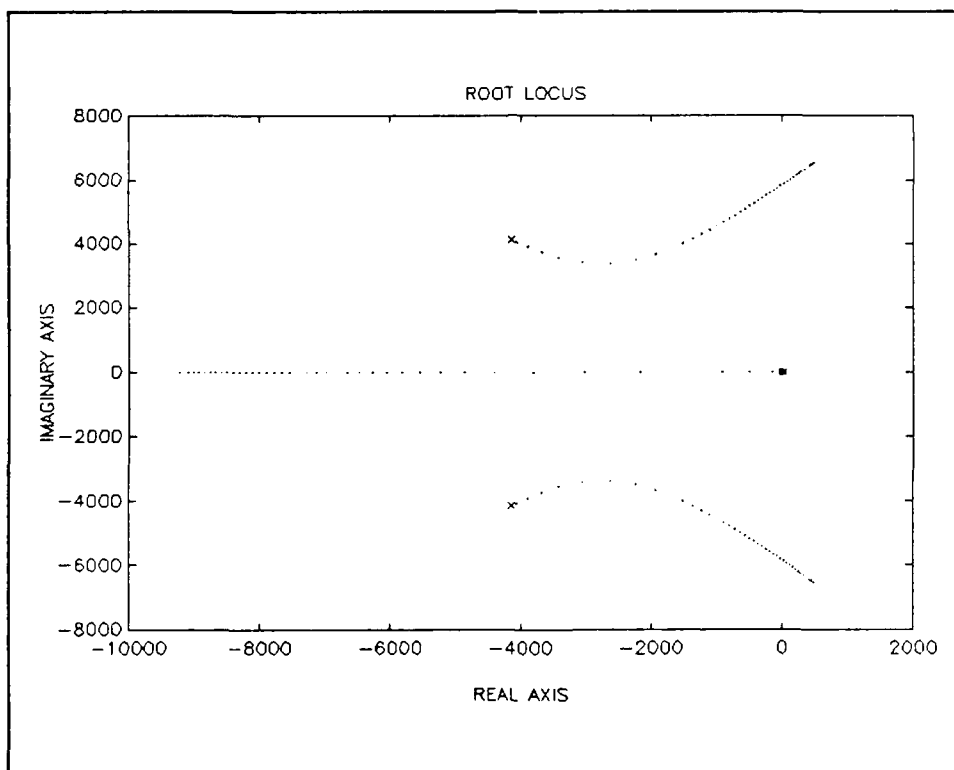


**Figure 3.8** Root Locus for the LQG Design with LTR for the Colocated System

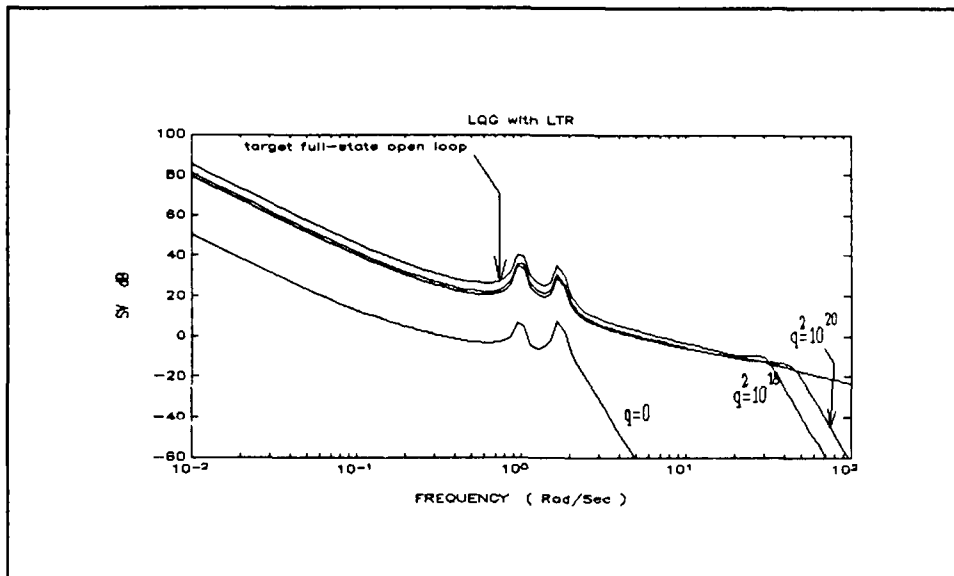


**Figure 3.9** LTR for the Non-located System

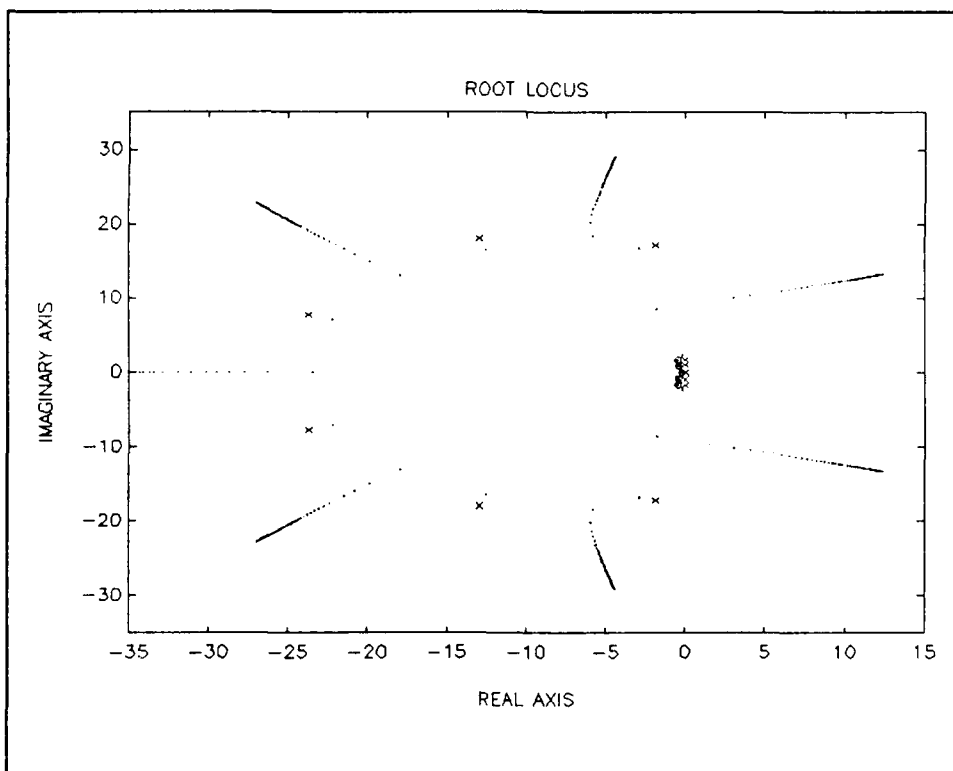


**Figure 3.10** Root locus for the LQG desing without LTR for the non-located system

### 3.8 STEP RESPONSE

The unit step input will now be applied to the closed loop full state regulator. The unit step input response is useful for analyzing the performance characteristics of a system. The time response is useful in revealing the rise time, settling time, and the steady state value [9:40].

The RHP zero has an interesting influence on the step response. Reid states that for non-minimum phase systems the initial response is negative. This means the system moves in the opposite direction in relation to the final steady-state value. If the system has no zeros (i.e. the non-colocated three element mass model), the initial response will be flat. The plot of the step response for the colocated and non-colocated systems are shown in Figure 3.11. The non-colocated system shows a flat response initially since it has no zeros. The colocated step response shows it fluctuates as it comes to its steady-state value. This is the result of the imaginary zeros and because the poles are lightly damped.

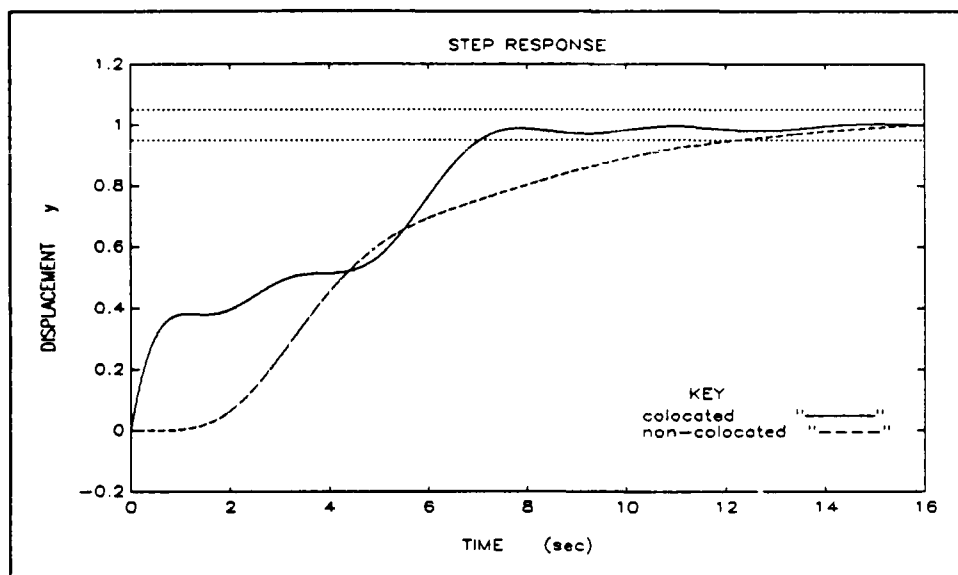


**Figure 3.11.** Step Response of the Three Element Model

### 3.9 CONCLUSION

The colocated LQG/LTR system is very robust to gain variations. However, the robustness decreases for  $q^2 = 10^9$  through  $10^{12}$ . The RMS response at these fictitious noise values show that the colocated system is much higher than the non-colocated system. While the non-colocated case has low RMS response, it is not robust in comparison to the colocated system. It does improve slightly for very large  $q^2$  values. See Table A.1 in Appendix A. Looking at the closed loop bandwidths show that the non-colocated system has very good damping and has the desirable high frequency roll off. The colocated system has little damping of its flexible poles. In this regard the non-colocated case is better.

The step response to the unit input also shows the non-colocated system has better damped poles and a smoother rise time curve. However, the system exhibits non-minimum phase behavior of having no initial response to the input for the first two seconds. See Figure 3.11. This may be an unacceptable response. Recall this single motion DOF model did not have RHP zeros to cause a negative response typical of non-minimum phase systems. This leads to the next chapter which shows that non-colocated systems have RHP zeros for two-motion DOF models.

Observing the closed loop eigenvalues of the LQG/LTR controller showed how it becomes robust. LQG design is helped by LTR because as the fictitious noise is increased, the compensator poles move toward the open loop plant zeros to notch them out. The Kalman filter accomplishes this task since its closed loop poles ( $A - K_f C$ ) at high  $q^2$  values moves right onto the plant zeros. On the other hand, the compensator zeros move toward the stable poles of the closed loop regulator ( $A - EK_c$ ). Thus, the plant poles during compensated feedback must move toward the compensator zeros which guarantees the stability and the robustness of the closed loop full-state regulator. In essence, the LQG compensator inverts the nominal plant and substitutes the desired LQR dynamics.

To summarize for the three element model using an initial noise intensity of  $Q_0 = 10^2$ , the colocated system can be made

robust by just using the LQG compensator; whereas, the non-colocated system can be improved slightly with LTR. To get better rise time curve and damping for the colocated system requires a lower bandwidth away from its low frequency imaginary zeros and therefore a drop in performance. On the other hand, the non-colocated system can achieve a higher bandwidth and better damping since it has no imaginary zeros affecting the crossover frequency it can attain.

#### IV. A TWO MOTION DEGREE OF FREEDOM SYSTEM

##### 4.1 Introduction

The first example presented in this thesis of the three element lumped mass system showed the non-colocated system was technically minimum phase (i.e. no zeros in the right half plane). However, the system showed non-minimum phase characteristics. For instance, the step response had initial flat response characteristic of a non-minimum phase system with no zeros. Loop transfer recovery to the full-state loop shape was limited, especially in comparison to the colocated loop recovery shapes. At high frequencies, it exhibited the characteristic steep roll-off of a non-minimum phase system.

##### 4.2 EXACT SOLUTION OF A TRANSVERSE BEAM

The three element lumped mass model is a single motion DOF system since it only has plane rotation about one axis. The numerator of the non-colocated transfer function was zeroth order and had no roots (refer to section 2.3.2). Thus, a single motion DOF system will not yield any zeros in the RHP. Therefore, a two motion DOF system will be examined to

demonstrate the non-minimum phase behavior for non-colocated structures. A two-dimensional beam which can translate and rotate will be needed. As shown in Reference 14 by Bryson and Wie, a Bernoulli-Euler beam with transverse bending vibrations will have zeros in the RHP [14:165].

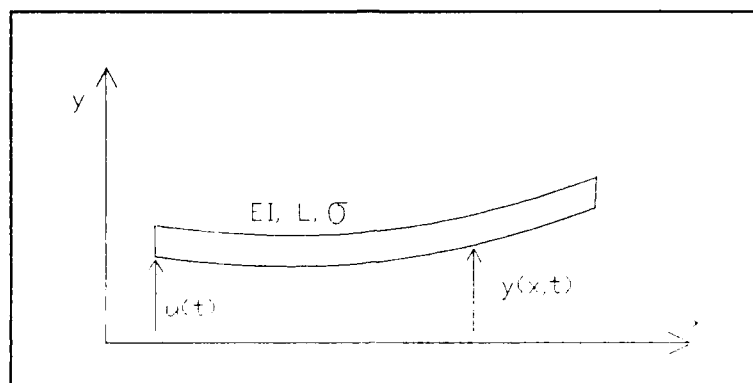


Figure 4.1 Free-free Transverse Beam

The equation of motion for the transverse beam is

$$y^{(iv)}(x, t) + \ddot{y}(x, t) = 0$$

(4.1)

$$\text{where } y^{(iv)} \triangleq \frac{\partial^4 y}{\partial x^4} \quad \text{and} \quad \ddot{y} \triangleq \frac{\partial^2 y}{\partial t^2}$$

and  $y(x, t)$  is the transverse displacement.

The displacement variables  $x$  and  $y$  are in units of  $L$ , time in units of  $(\sigma L^4/EI)^{1/2}$ .  $\sigma$  is the mass density per unit length. Taking the Laplace transforms of Eqn 4.1 yields

$$y^{(iv)}(x,s) + s^2 y(x,s) = 0 \quad (4.2)$$

Thus the transcendental transfer functions for free-free boundary conditions for the two cases of colocation and non-colocation yields the following

$$\frac{y(0,s)}{u(s)} = \frac{\sinh\lambda\cosh\lambda - \cosh\lambda\sinh\lambda}{\lambda^3 (1 - \cos\lambda\cosh\lambda)} \quad (4.3a)$$

$$\frac{y(1,s)}{u(s)} = \frac{\sinh\lambda - \sin\lambda}{\lambda^3 (1 - \cos\lambda\cosh\lambda)} \quad (4.3b)$$

where  $\lambda^4 = -s^2$  or  $s = j\omega$  (in the frequency domain)

Solving for Eqn 4.3a directly shows the poles and zeros alternating on the imaginary axis of the complex plane as shown in Figure 4.2. The non-located case, Eqn 4.3b, has infinite number of reflexive zeros on the real axis as shown in Figure 4.3.

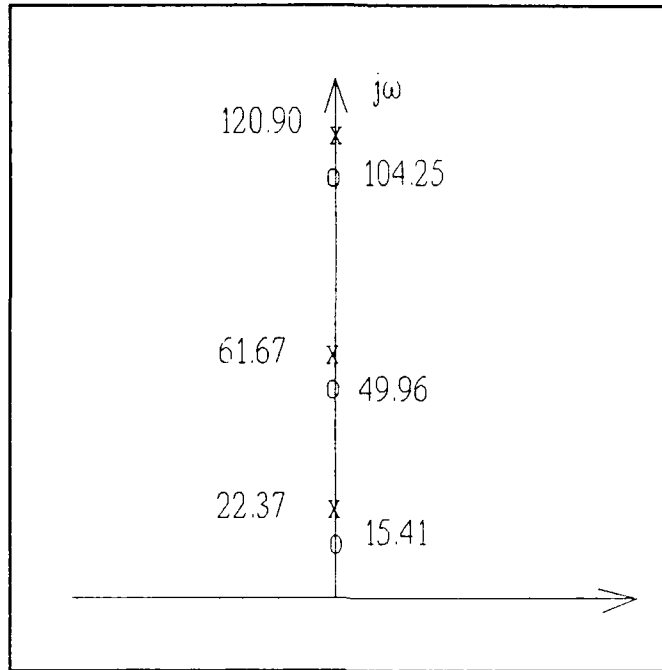


**Figure 4.2** Exact Poles/Zeros of a Colocated System

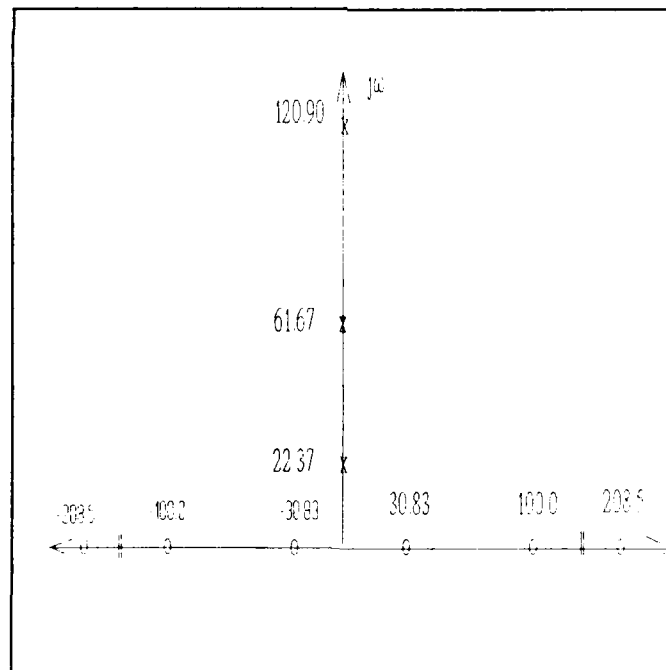


**Figure 4.3** Exact Poles/Zeros of a Non-colocated System

#### 4.2.1 MODAL TRUNCATION AND ITS EFFECT ON ZERO LOCATION

Eqn 4.3 for the closed form solution to the Bernoulli-Euler beam shows that non-colocated structures have RHP zeros on the real axis. When the model is truncated, the finite dimensional form of the transfer function derived from Eqn 2.1 shows that there can be complex zeros as well.

$$\frac{y(1, s)}{u(s)} = -\frac{2}{s^2} + \sum_{i=1}^N \frac{4(-1)^{i+1}a_i}{s^2 + \omega_i^2} \quad (4.2)$$

Reference 14 shows that Eqn 4.4 yields zeros on the real axis of the RHP when  $N = 1$ . When  $N = 2$ , Eqn 4.4 yields complex zeros in the RHP. Thus, a truncated model will not necessarily have all its zeros on the real axis. But, it will have RHP zeros.

#### 4.3 APPROXIMATE SOLUTION BY FINITE ELEMENT METHOD

Using partial differential equation representation for structures can be difficult to solve; therefore, the Finite Element Method (FEM), will be used to analyze a two motion DOF beam. The author used the FEM computer program, ANSYS, to solve for the eigenvectors and the eigenvalues needed to get

the equations of motion (EOM).

Using the finite element approach as presented by Meirovitch [8:ch.4], the general EOM for an undamped system is

$$[m]\{\ddot{q}(t)\} + [k]\{q(t)\} = \{Q(t)\} \quad (4.5)$$

where  $[M]$  and  $[K]$  are constant mass and stiffness matrices of size  $n$  (number of modes used)  
 $\{q\}$  and  $\{Q(t)\}$  are the column matrices of generalized coordinates and generalized forces, respectively.

Eqn 4.4 is difficult to solve because of the coupling in the mass and the stiffness matrices. To solve these linear 2nd order equations, the linear transformation

$$\{q(t)\} = [u]\{\eta(t)\} \quad (4.6)$$

where  $\{\eta(t)\}$  is a new set of generalized coordinates,  
 $[u]$  is a transformation matrix or a modal matrix comprised of the eigenvectors,

is used to decouple the mass and stiffness matrices so that they are diagonalized. The EOM using the new generalized coordinates is

$$[m][u]\{\ddot{\eta}(t)\} + [k][u]\{\eta(t)\} = \{Q(t)\} \quad (4.7)$$

Pre-multiplying by  $[u]^T$  results in the modal EOM

$$[M]\{\ddot{\eta}(t)\} + [K]\{\eta(t)\} = \{N(t)\} \quad (4.8)$$

where  $[M] = [u]^T[m][u]$  is the modal mass matrix,  
 $[K] = [u]^T[k][u]$  is the modal stiffness matrix.

Orthogonality of the modal matrices diagonalize the mass and the stiffness matrices (given that they are constant and symmetric). It is common to normalize the mass matrix to an identity matrix. Multiplying by the inverse of the identity mass matrix makes the stiffness matrix equal to the eigenvalues since  $\omega^2 = K/M$ . The final form of the EOM is then

$$[I]\{\ddot{\eta}(t)\} + [\omega^2]\{\eta(t)\} = \{N(t)\} \quad (4.9)$$

This form of the EOM is readily available from finite element computer programs such as ANSYS. Eqn 4.8 can be put into the state-space form of Eqn 2.8

$$\dot{x} = \begin{bmatrix} 0 & I \\ -[\omega^2] & 0 \end{bmatrix} \begin{Bmatrix} \eta \\ \dot{\eta} \end{Bmatrix} + \begin{bmatrix} 0 \\ U^T Q \end{bmatrix} u \quad (4.10)$$

where  $u$  is the input control force,

Linear transformation must also be applied to  $y = Cx$  to get the output matrix in the state space equation form.

$$y = \underline{C}[u][\eta \ \dot{\eta}]^T \quad (4.11)$$

Thus, the state space equation for output becomes

$$y = [ \underline{C}[u] \quad | \quad 0 ] x$$

The matrix  $C$  is padded with zeros to match the size of the state vector  $x$  (since no velocity measurements are taken). The  $\underline{C}$  matrix in Eqn 4.11 for a single output case will be a row matrix of size  $1 \times n$  with ones at the nodes of interest.

#### 4.4 TEN ELEMENT TRANSVERSE BEAM EXAMPLE

To show that the FEM can produce the  $[A]$ ,  $[B]$ , and  $[C]$  matrices required for the state-space equations, a ten element transverse beam is modelled in ANSYS. See Appendix B for the ANSYS data input file.

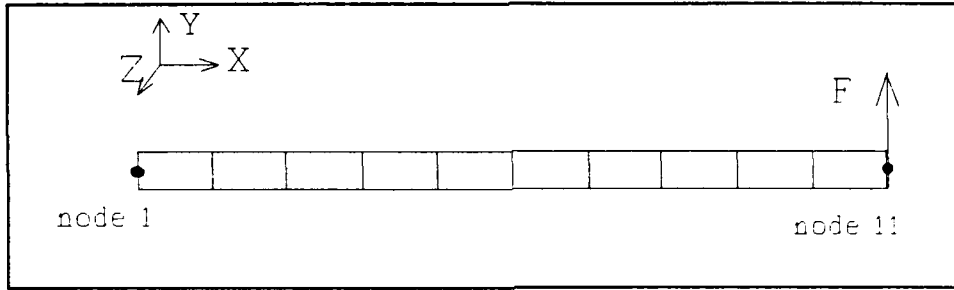


**Figure 4.4** Ten Element Transverse Beam

The two dimensional beam element (STIF 3) is an uniaxial element with tension-compression and bending capabilities. It has three DOF at each node: translation in the x and y direction; and rotation about the z axis.

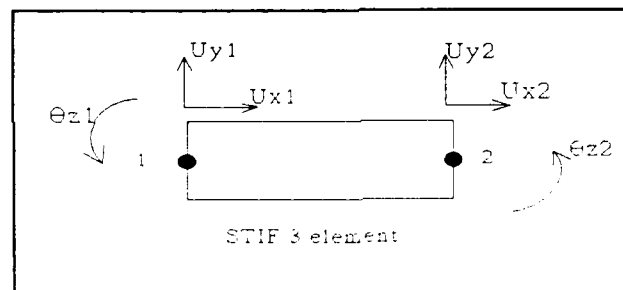


**Figure 4.5** DOF for the Two Dimensional Element

For this example problem because bending is the primary mode of interest, x translational DOFs were neglected. The ten element beam has a total of 40 DOF (4 DOF/element x 10 elements). Eliminating the DOFs at the internal nodes due to the constraints results in total of 22 unknown DOF. Solving this free-free beam using modal analysis in ANSYS produces a

22x22 modal matrix,  $[u]$ , associated with the DOF

$$DOF = \begin{Bmatrix} u_{y1} \\ \theta_{z1} \\ \vdots \\ u_{y11} \\ \theta_{z11} \end{Bmatrix}$$

The A matrix is formed from the mass and stiffness matrices, but ANSYS has normalized the mass matrix to identity so that A can be derived by Eqn 4.9. The A matrix is

$$A = \begin{bmatrix} 0^{22 \times 22} & I^{22 \times 22} \\ -[\omega^2]^{22 \times 22} & 0^{22 \times 22} \end{bmatrix}$$

ANSYS outputs the eigenvalues in natural frequencies in units of cycles per time and must be converted to radians per time before using in the A matrix. Listed in Table 4.1 are the eigenvalues from Ansys compared to the closed form solution for free-free transverse beams [14:275].

**Table 4.1** Eigenvalues from Ansys and the Closed Form Solution

<u>Ansys</u>		<u>Closed Form Solution</u>	<u>Error</u>
0.0	Hertz	0.0	0.0 %
0.0		0.0	0.0
4.072		4.088	0.4
11.196		11.259	0.6
21.884		22.080	0.9

Note the first two modes are the rigid body modes ( $\lambda = 0.0$ ). The error is less than one percent for the first five modes, which shows the accuracy of the model with the full twenty-two modes. Later section will compare the eigenvalue solution for just four modes. The Q force matrix is

$$Q = \begin{bmatrix} 0 \\ 0 \\ 0 \\ \vdots \\ 1 \end{bmatrix}$$

where 1 has been placed at the 21st row representing node 11 in the y direction. Therefore the B matrix is

$$B = \begin{bmatrix} 0 \\ --- \\ U^T Q \end{bmatrix}$$

where  $U^T Q$  is the 21st row of the transposed modal matrix. The output matrix is

$$C = \begin{bmatrix} 1 & 0 & 0 & 0 & \dots & 0 & 0 \\ 0 & 0 & 0 & 0 & \dots & 1 & 0 \end{bmatrix}$$

where the ones represent a displacement sensor at node 1 (non-colocated) and node 11 (colocated). Remembering

$$C = [\underline{C}[u]^{(2 \times 22)} \quad | \quad 0^{(2 \times 22)}]$$

where  $\underline{C}[u]$  becomes the 1st row and the 21st row of the modal matrix,  $[u]$ .

#### 4.4.1 MODEL REDUCTION TO FOUR MODES

Because of the large size of the  $A$  matrix (44x44), the model was reduced to only the first four modes. For the ten element beam, going from twenty-two to four modes still produced accurate results for the first two flexible poles. This is evident by examining Figures 4.6 and 4.7. The Bode plot of the reduced beam with four modes is compared with the frequency response spectrum from ANSYS (KAN 6 Analysis). In this way, two different methods are used to find the transfer function between input and output for a beam.

The reduction produced a 8x8  $A$  matrix containing the mode shapes of interest. The first four eigenvalues are still very accurate to the closed form solution shown in Table 4.1.

$\lambda$	=	0.0	Hertz
		$0.871e-6$	
		4.232	
		12.727	

The second mode is the rigid body rotation, so the value was made zero. The first flexible pole is accurate to within 3.5 percent of the closed form solution. See Figure 4.8 for the mode shapes associated with the eigenvalues.

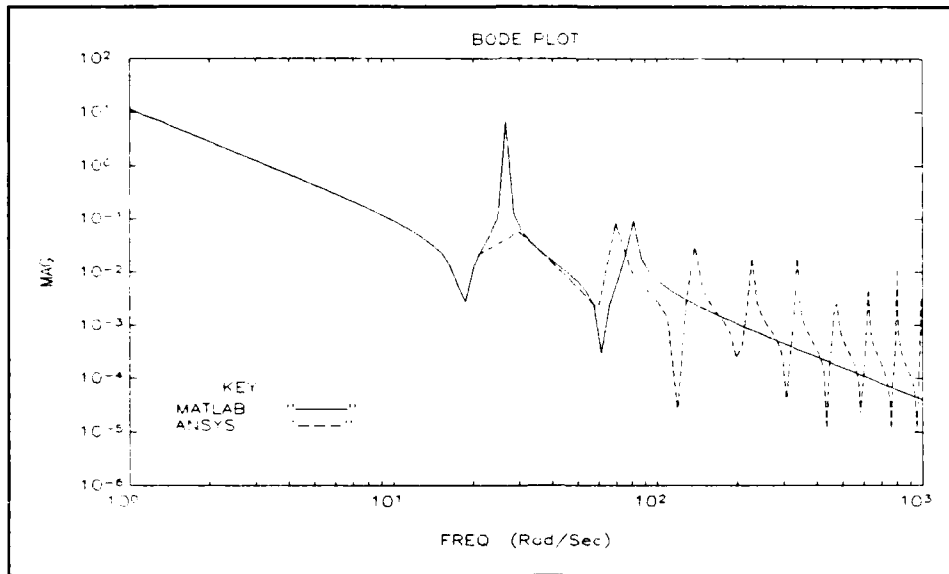


**Figure 4.6** Bode Plot Comparing Frequency Response of 11 Modes to the Reduced 4 Modes for the Colocated Beam

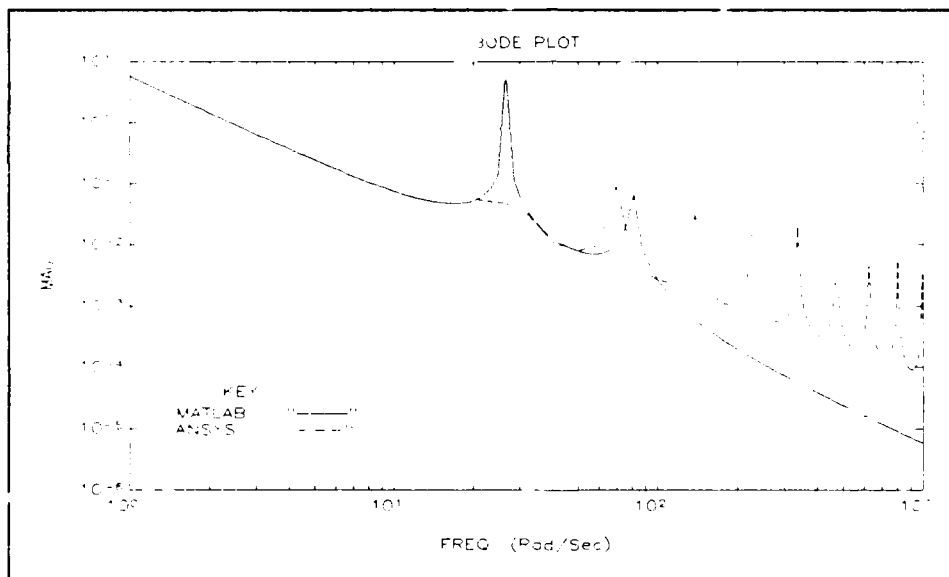


**Figure 4.7** Bode Plot Comparing the Frequency Response of 11 Modes to the Reduced 4 Modes for the Non-colocated Beam

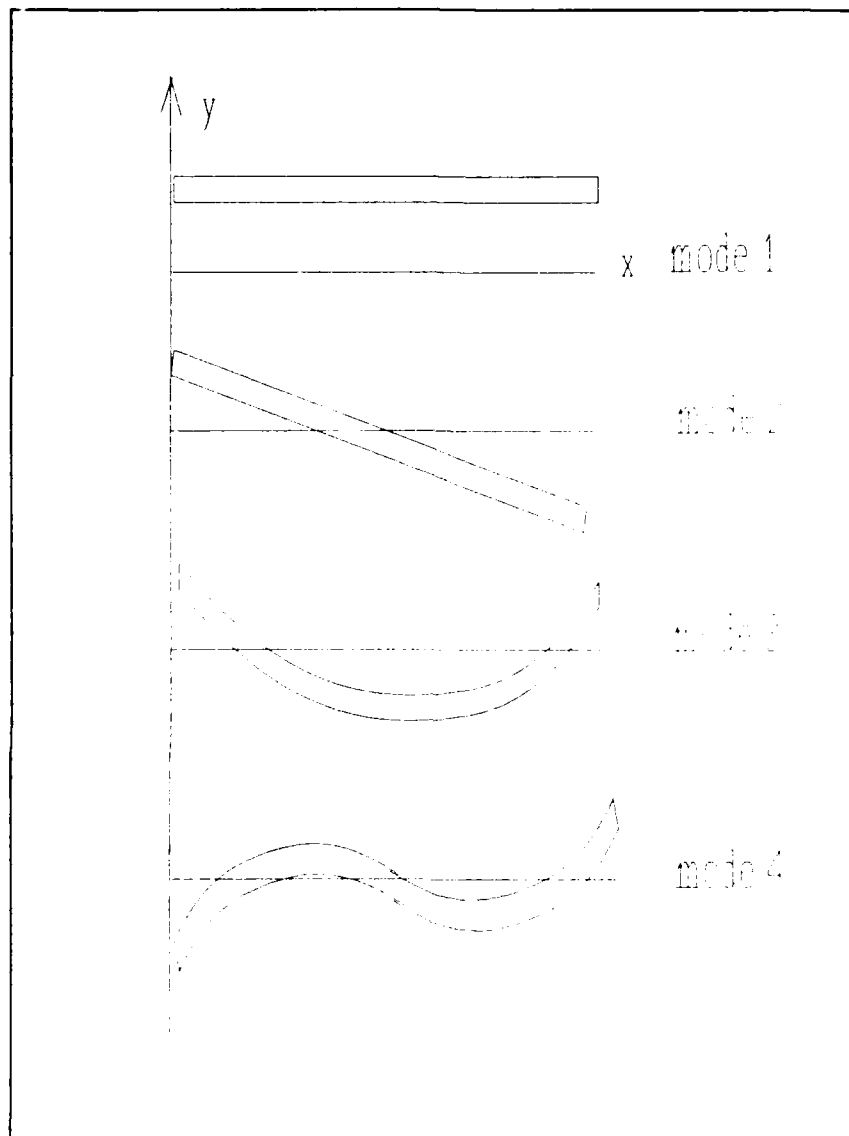


**Figure 4.8** The Four Mode Shapes of the Ten Element Beam

The final A matrix is

$$A = \begin{bmatrix} 0 & 0 & 0 & 0 & 1 & 0 & 0 & 0 \\ 0 & 0 & 0 & 0 & 0 & 1 & 0 & 0 \\ 0 & 0 & 0 & 0 & 0 & 0 & 1 & 0 \\ 0 & 0 & 0 & 0 & 0 & 0 & 0 & 1 \\ 0 & 0 & 0 & 0 & 0 & 0 & 0 & 0 \\ 0 & 0 & 0 & 0 & 0 & 0 & 0 & 0 \\ 0 & 0 & -7.06 \times 10^2 & 0 & 0 & 0 & 0 & 0 \\ 0 & 0 & 0 & -6.39 \times 10^3 & 0 & 0 & 0 & 0 \end{bmatrix}$$

The B matrix is

$$B = \begin{bmatrix} 0 \\ 0 \\ 0 \\ 0 \\ 3.288 \\ 0.727 \\ 3.393 \\ 4.128 \end{bmatrix}$$

The C matrix is

$$C = \begin{bmatrix} 3.288 & 0.727 & 3.393 & 4.128 & 0 & 0 & 0 & 0 \\ -2.272 & 2.485 & 3.654 & -3.011 & 0 & 0 & 0 & 0 \end{bmatrix}$$

The eigenvalues of the A matrix are the system poles and the transmission zeros are found using the tzero command in MATLAB. They are listed in Table 4.2.

**Table 4.2** Poles and Zeros of the Ten Element Beam

<u>Poles</u>	<u>Colocated Zeros</u>	<u>Non-colocated Zeros</u>
0,0,0,0 r/s	0,0	0,0
$\pm 26.59i$	$\pm 18.32i$	$\pm 32.52$
$\pm 79.97i$	$\pm 61.89i$	$\pm 65.20$

Note the extra pair of zeros for the second rigid body motion is canceled by the pair of zeros for the colocated and non-colocated zeros. This pole/zero cancellation did not cause observability problems. Shown below is the Bode plot of the open loop plant for both the colocated and non-colocated systems. Note the dips in the colocated plot indicating it has imaginary zeros;whereas, the non-colocated has no dips because its zeros are on the real axis. The non-colocated low frequency gain is little less than the colocated gain;therefore, a pre-filter gain of 2 is required to the input of the B matrix to make the two systems equal for comparison purposes.

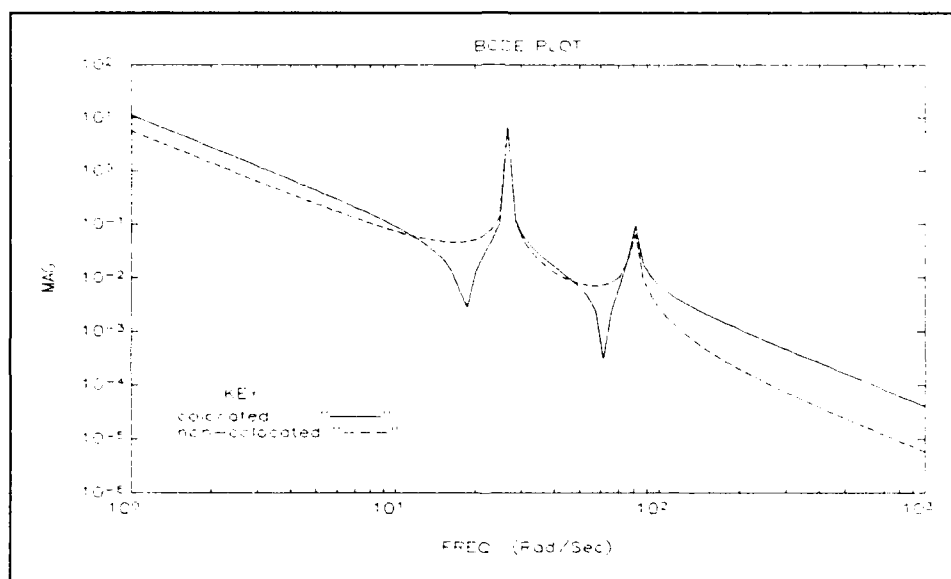


**Figure 4.9.** Bode Plots of the Colocated and Non-colocated Ten Element Beam

#### 4.5 LQG/LTR CONTROL DESIGN ON THE BEAM

The control design on the transverse beam produced interesting results. The control design without LTR (the fictitious noise parameter  $q = 0$ ), resulted in the colocated system being robust to large gain variations (from 0.5 to 43). The non-colocated system did not improve with LTR as expected of a non-minimum phase system.

Both systems were designed to have the same bandwidth of about 8 rad/sec. Figure 4.10 represents the Bode plot of the closed loop bandwidths for both cases. The weighting matrices used for the LQR for the colocated case is

$$Q_c = \text{diag}(10^5 \ 10^5 \ 10^5 \ 10^5 \ 10^3 \ 10^3 \ 10^3 \ 10^3),$$

and for the non-colocated case is

$$Q_c = \text{diag}(10^{4.5} \ 10^{4.5} \ 10^4 \ 10^4 \ 10^3 \ 10^3 \ 10^3 \ 10^3).$$

For both cases, the noise intensity at the input for the LQE was selected as

$$Q_o = 10^5.$$

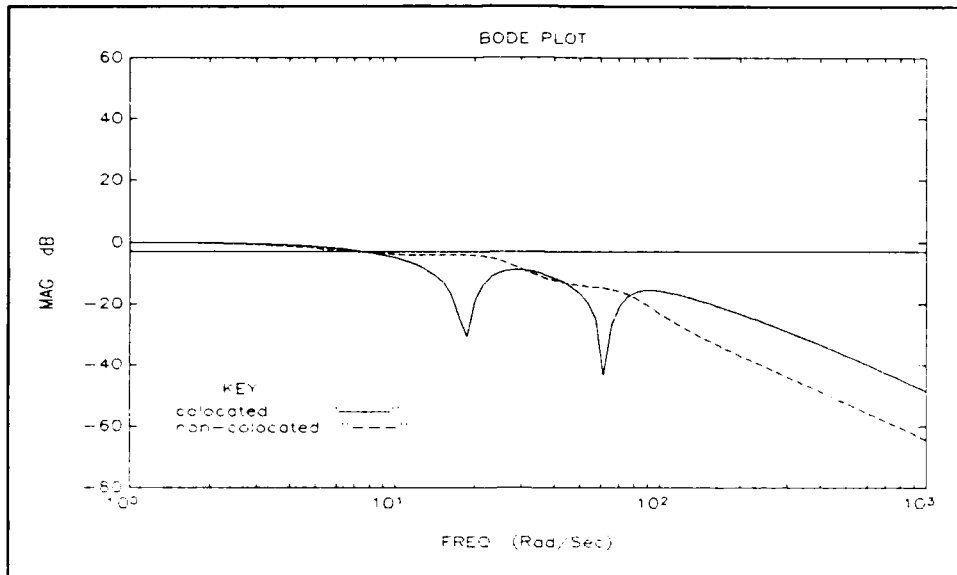


**Figure 4.10** Closed Loop Bandwidths for the Ten Element Beam

The root locus plots show the poles of the closed loop system as gain is varied. The collocated system went unstable at gain of  $k = 43$ . See Figure 4.11. This system became less robust after LTR for  $q^2 = 10^9$ . Then the system started to increase in robustness until the gain value exceeded 100. Observing the LTR plots of Figure 4.13 clearly shows that the system gained the robustness of a full-state regulator. See Table A.2 in Appendix A for the results from the design iterations. Figures 4.14 shows the root locus plot for  $q^2 = 10^{12}$ . Note the highest frequency pole is the one that goes unstable. So, this system is very robust for the lower frequency poles.

The non-colocated case was not able to get full loop recovery no matter how much fictitious noise was added. In fact, gains after  $q = 10^{12}$  made no improvement on the low frequency recovery. See Figure 4.15 for the LTR plots. The poles became unstable after a gain of  $k = 2$  for all  $q^2$  values. See Table A.2 in Appendix A. The root locus plot for  $q^2 = 10^{12}$  is shown in Figure 4.16. This plot clearly shows the poles moving toward the right half plane zeros.

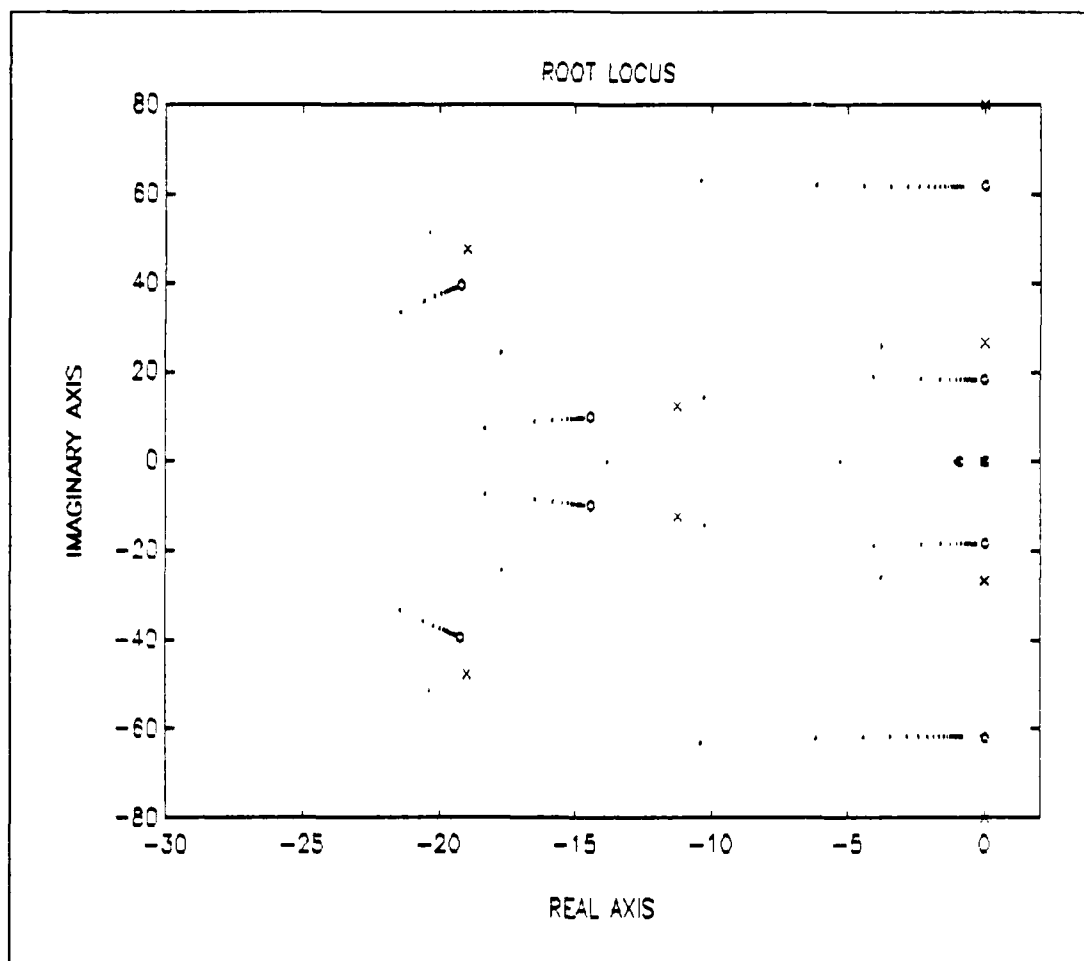


**Figure 4.11** Root Locus for the LQG Design Without LTR for the Colocated System

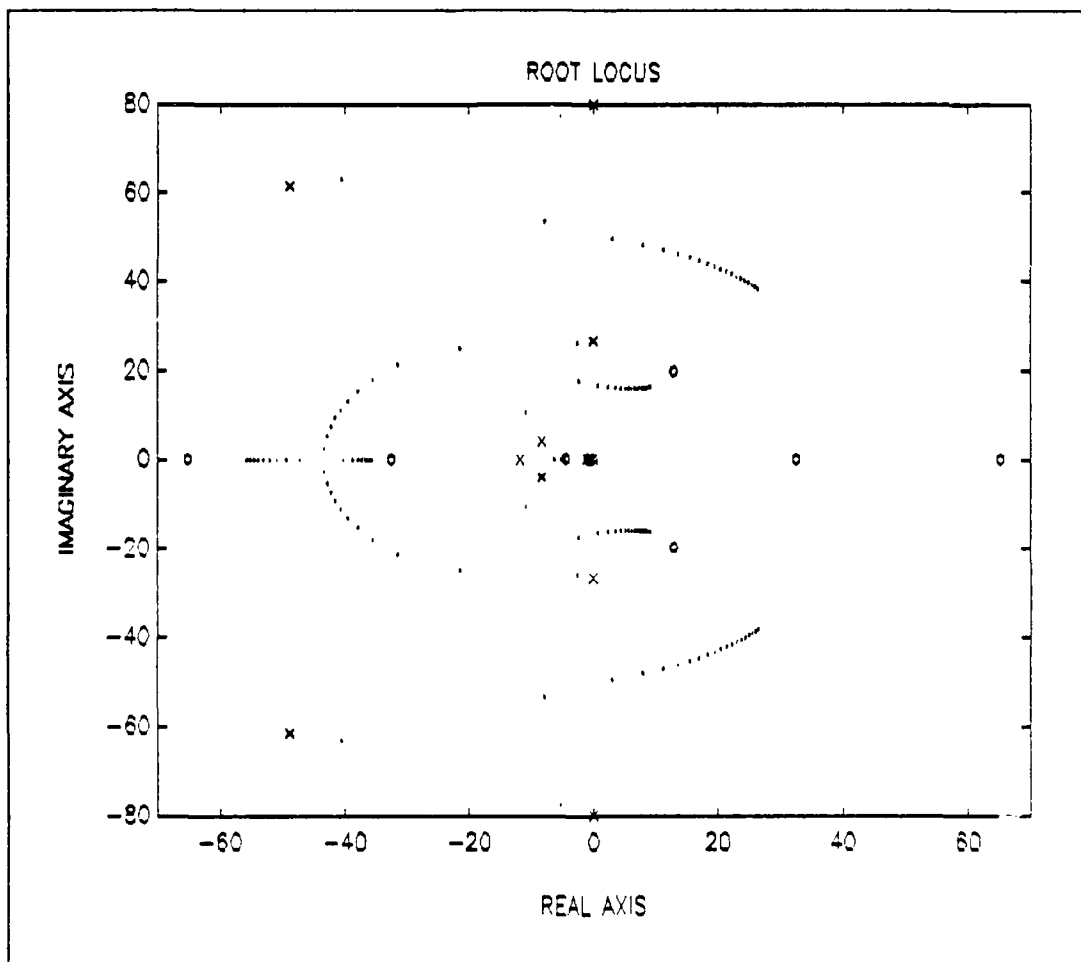


**Figure 4.12** Root Locus for the LQG Design Without LTR for the Non-colocated System.

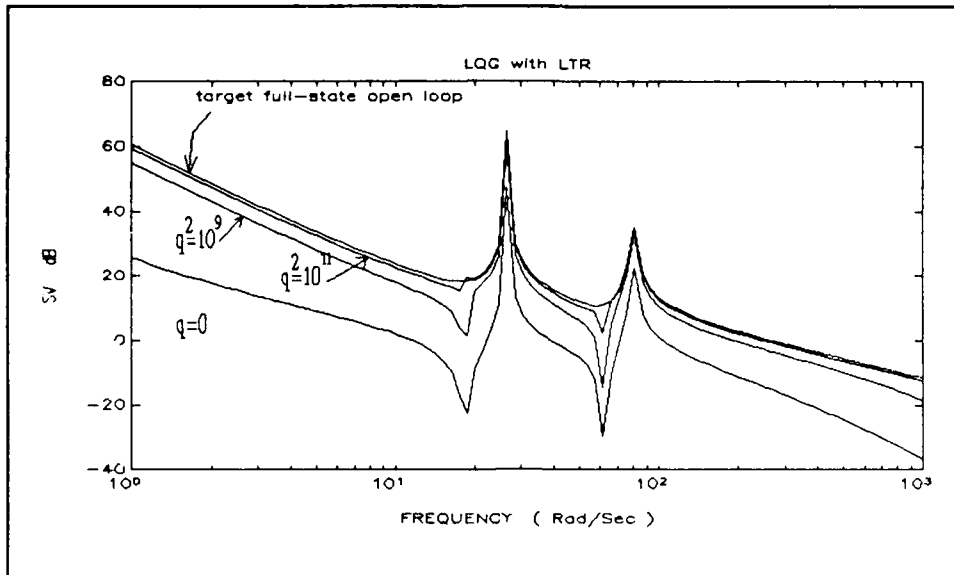


**Figure 4.13** LTR for the Colocated System

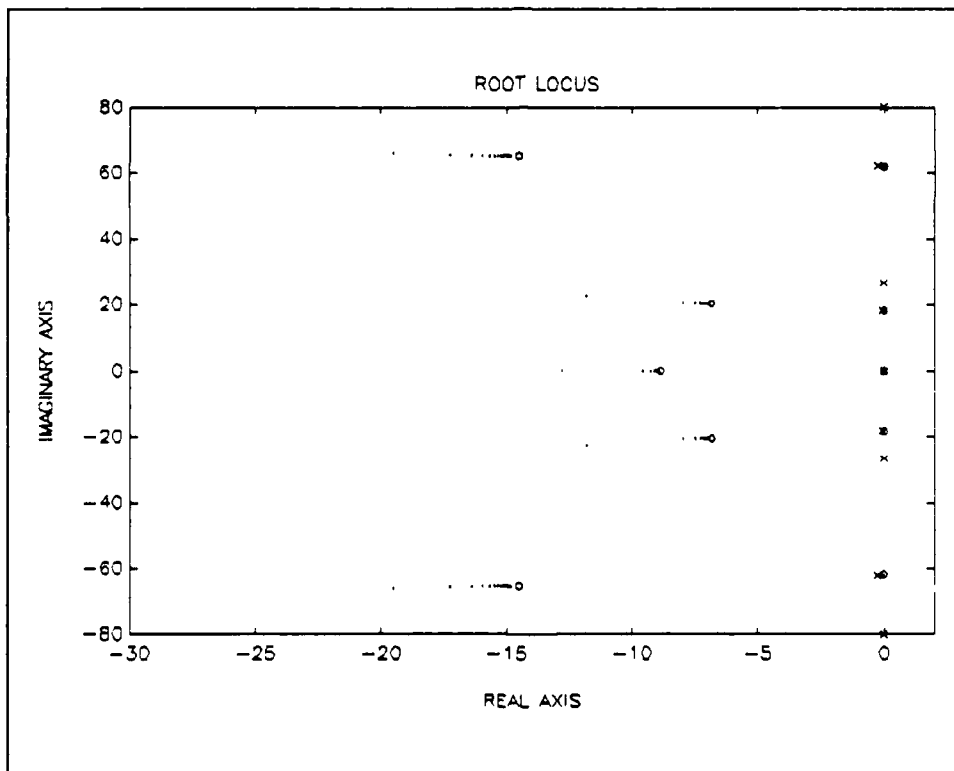


**Figure 4.14** Root Locus for the LQG Design with LTR for the Colocated System

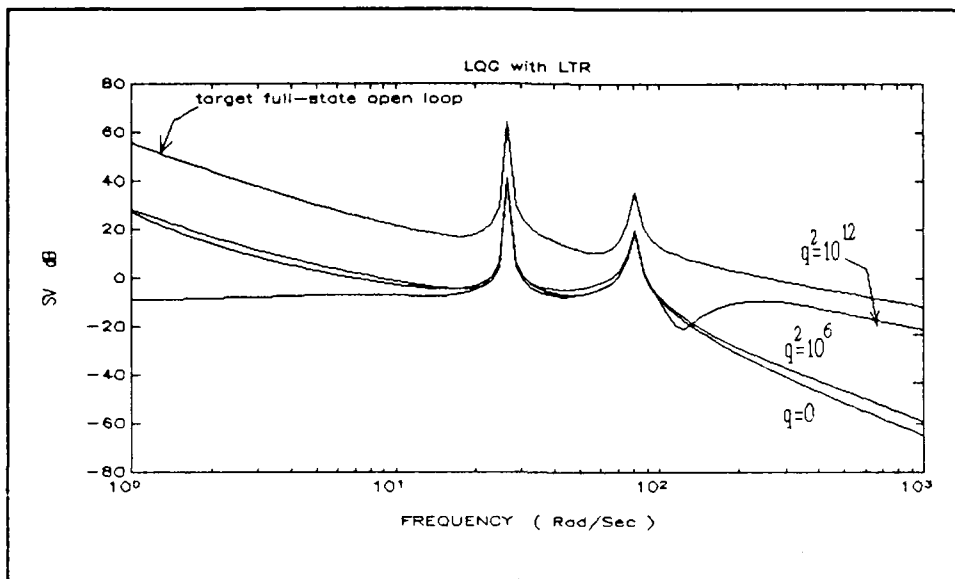


**Figure 4.15** LTR for the Non-colocated System

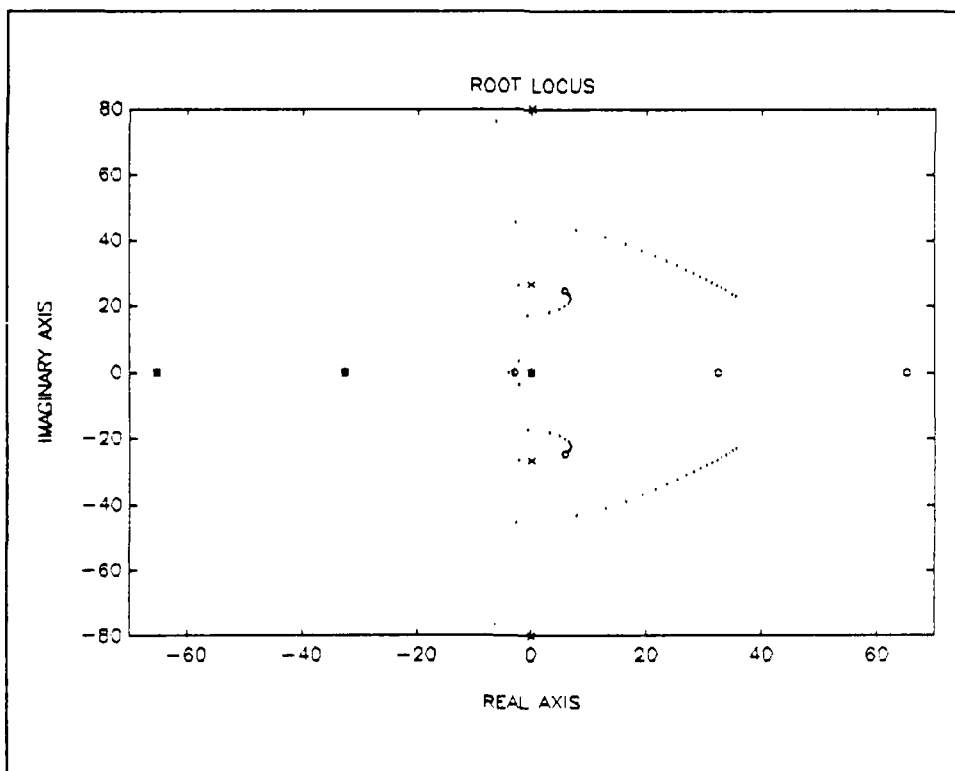


**Figure 4.16** Root Locus for the LQG Design with LTR for the Non-colocated System

#### 4.5.2 STEP RESPONSE

The step response plot clearly shows which system is non-minimum phase. The non-colocated system has an initial negative response to the step input. Otherwise, this system has much better damping than the colocated system which has ringing.

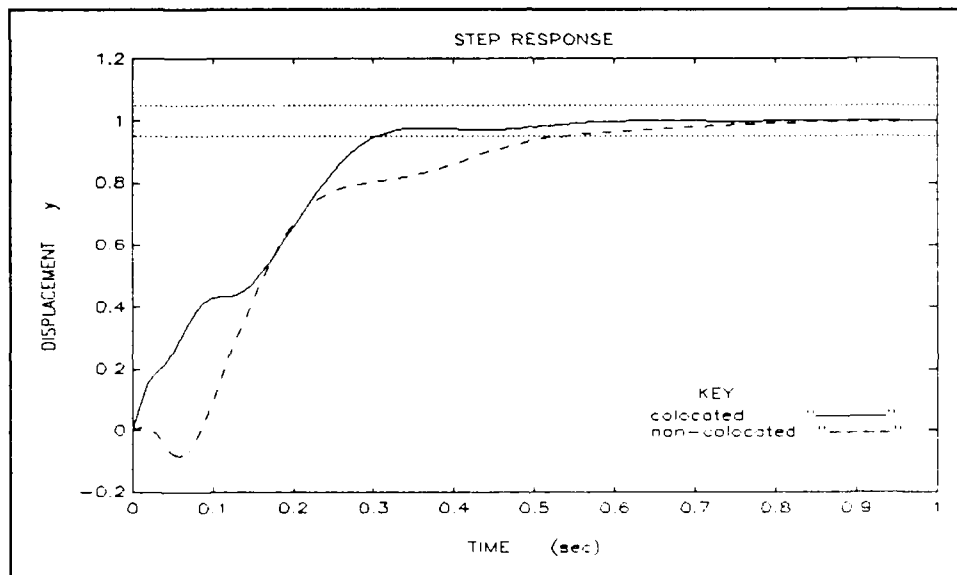


**Figure 4.17** Step Response of the Ten Element Beam

#### 4.6 CONCLUSION

For the ten element beam after large amounts of fictitious noise was added, the colocated system became very robust as it approached the target full-state regulator. On the other hand, the non-colocated system did not get any recovery for any value of fictitious noise. The RMS response of the colocated system was also much less than the non-colocated system. See Table A.2 in Appendix A.

The step response for both systems had similar results as the three element lumped mass example. The colocated system had ringing in its rise curve due to the lightly damped poles and the influence of the zeros on the imaginary axis. The non-colocated rise curve had the initial negative rise associated with the RHP zero.

Reviewing the closed loop pole locations show that LQG/LTR designs agree with theory. As  $q^2$  is increased for the colocated system, the Kalman filter's closed loop poles notches out the plant zeros. Meanwhile, the LQG/LTR compensator zeros move toward the closed loop poles of the full-state regulator. In turn, the root locus shows the plant's poles moving toward the compensator zeros during feedback. This is clear in Figure 4.15 of the non-colocated system which shows the filter poles notching out the plant zeros in the LHP. Thus, the compensated feedback system achieves the robustness of a full-state regulator. The non-

colocated system can not achieve loop recovery since it has RHP zeros which prevent the Kalman filter poles from notching out the zeros. However, the colocated system has higher noise which seems to cause the design trade-off in improving system robustness with LTR.

## V. FINITE ELEMENT MODEL OF CONTRAVES P52F GIMBALS

### 5.1 FINITE ELEMENT MODELING

The gimbal structure used in this investigation is a target motion simulator built by Contraves USA. This gimbal must be robust to parameter variations because it must accommodate many different types of missiles for testing. The control design must be able to handle the changes in the mass and inertia of the different payloads.

The gimbal has an inner (azimuth axis) and an outer (elevation axis) gimbal arrangement. The gimbal is driven by hydraulic actuators that provide torque and uses position and torque transducers (sensors). The torque for the finite element model is applied on a node on the inner gimbal at point A in Figure 5.1. Point A is also the location of the colocated sensor and Point B is the location for the non-colocated sensor. The two gimbals are connected together by a pipe element (STIF 12) with soft beam elements (STIF 3) representing the bearing connection that simulates the rotation of the inner gimbal. For this thesis, the outer gimbal was fixed against rotation. The model is three dimensional in that it has all six DOF (xyz translation and rotation) associated with the nodes.

The ANSYS model in Figure 5.1 has over one thousand elements. Because of the large number of modes available, the modal analysis used only the first five modes.

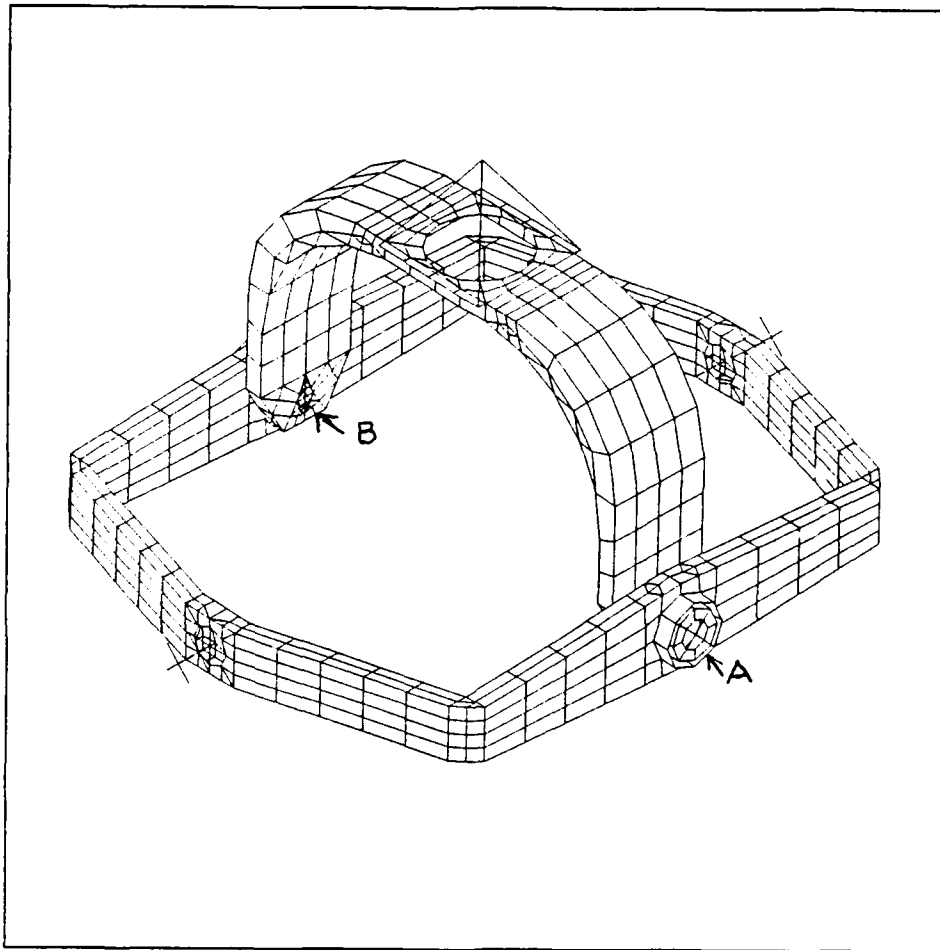


Figure 5.1 Contraves P52F Gimbal

This truncated model produced the following eigenvalues in its natural frequency form.

$\lambda =$  1.418 Hz  
 13.736  
 61.460  
 3940.861  
 4761.030

The first mode was found to be the rigid body mode of the inner gimbal. So, this frequency was taken as zero. The mode shape plot of Figure 5.2 shows the rotation (the solid shape) and the dotted line representing the original shape. The second mode caused a pole/zero cancelation and was omitted from the analysis. The last two eigenvalues are at very high frequencies. Thus, the only effective flexible pole is the third mode at 61.46 Hz or 386.2 rad/sec.

**Table 5.1** Poles and Zeros of the Contraves Model

<u>Poles</u>	<u>Colocated Zeros</u>	<u>Non-colocated Zeros</u>
0,0		
$\pm 386.2i$	$\pm 173.6i$	$\pm 229.7$
$\pm 24761.0i$	$\pm 2247.8i$	$\pm 8667.1$
$\pm 29914.0i$	$\pm 26915.0i$	$0.0 \pm 11631.0i$

Note Table 5.1 shows the non-colocated case has an imaginary zero. This is not that unusual and is the result of modal truncation. The bode plot shows the poles and zeros in Figure 5.3.

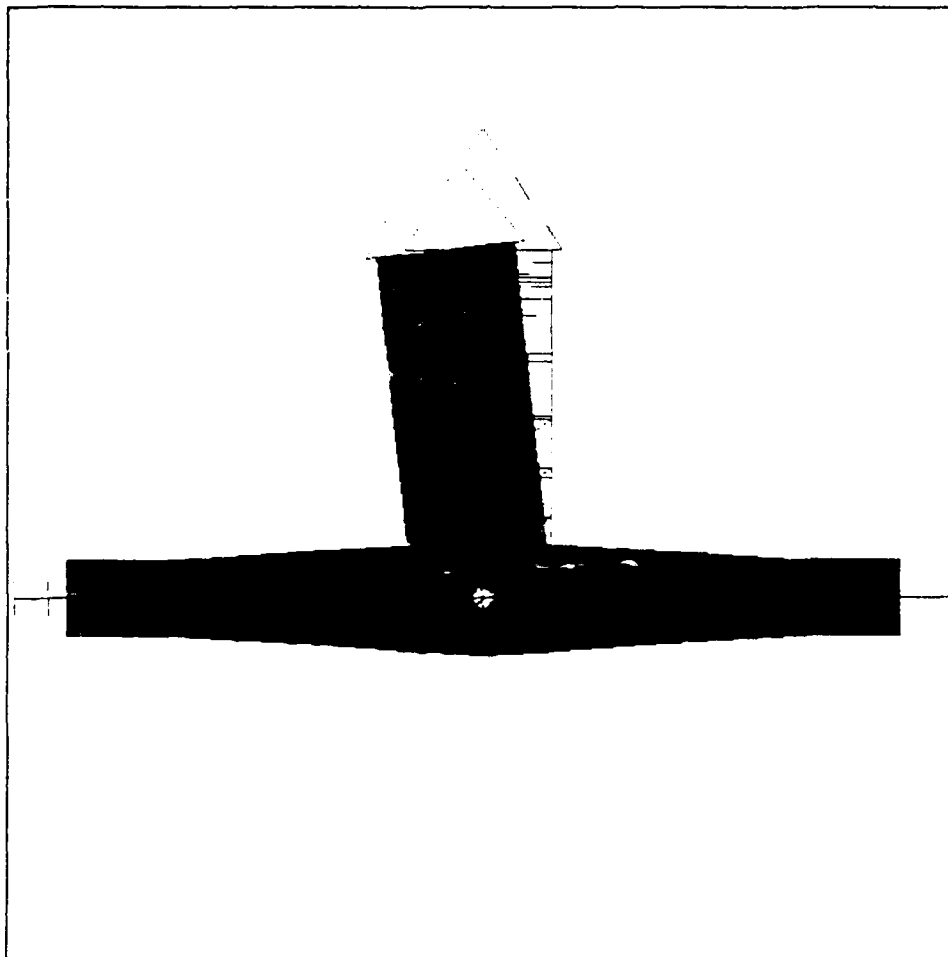


**Figure 5.2** The First Mode Showing the Rigid Body Rotation

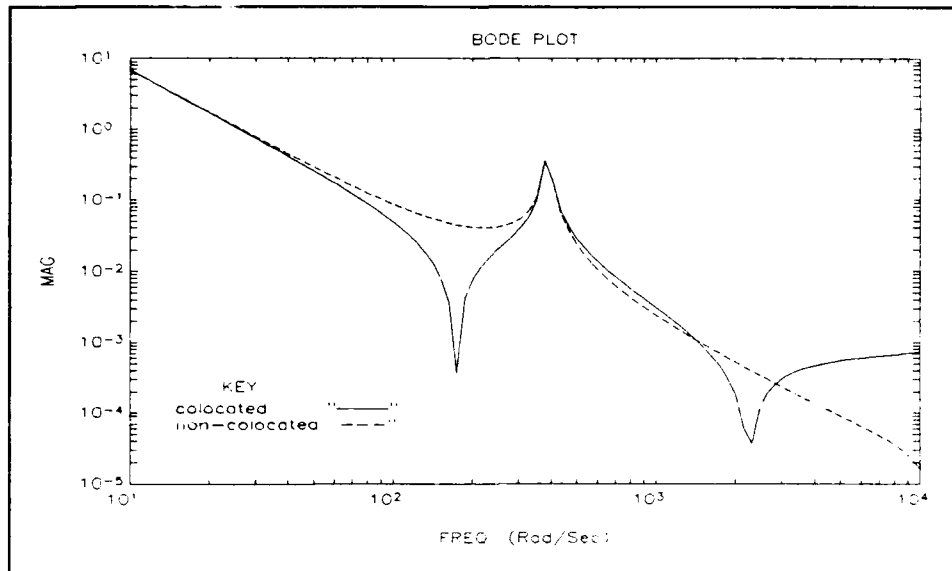


**Figure 5.3** Bode Plots of the Colocated and Non-colocated Contraves Model

The accuracy of the truncation compared to the frequency response of the structure shows the dominant pole at 386 rad/sec was matched very well. But, the frequency response shows there is also another pole/zero pair near 250 rad/sec that the truncated model does not have. See Figures 5.4 and 5.5 on the next page. Considering the fact this model has all six DOF and our sensor is only taking the rotational measurement, the author considers this to be an acceptable since the closed loop bandwidth is at 100 rad/sec which is below this first pole at 250 rad/sec. A position sensor located elsewhere on the model may sense the pole missed by the sensor located at points A and B in Figure 5.1. Then the control problem becomes single input and multi-output; but, this thesis is only examining the SISO case.

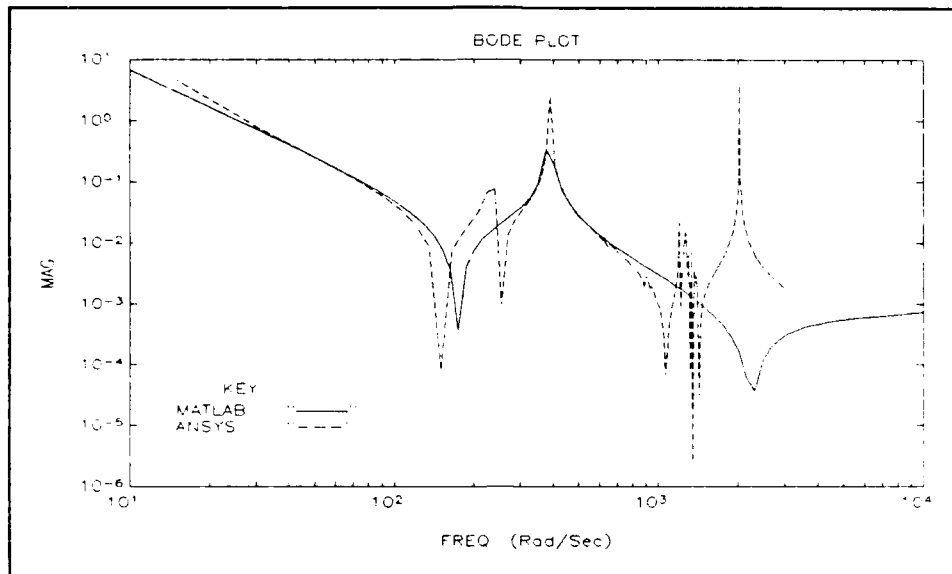


**Figure 5.4** Truncated Model Compared to the Frequency Response for the Colocated Case

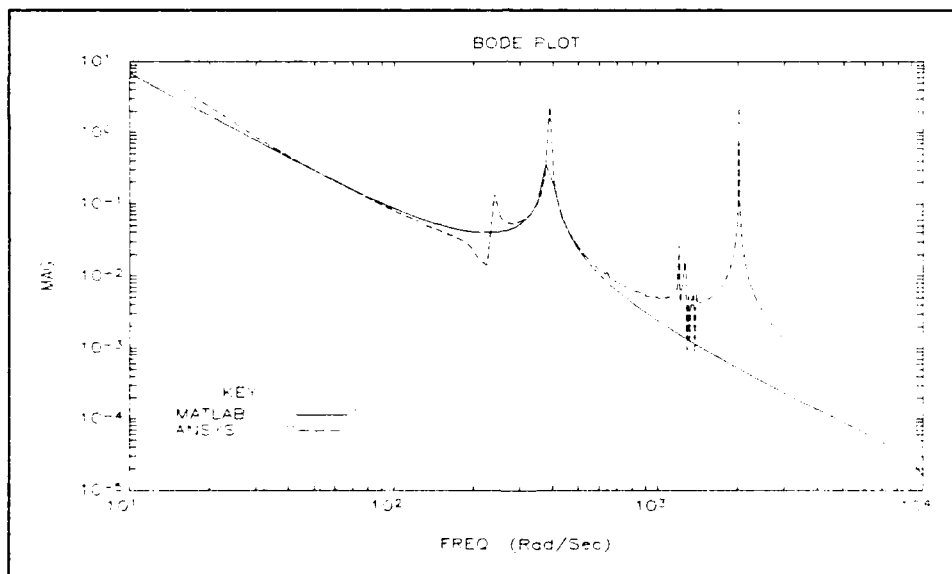


**Figure 5.5** Truncated Model Compared to the Frequency Response for the Non-colocated case

Further investigation was done to better match the frequency response curve by using a MATLAB script file ANSYS.M written by Professor Bradley Liebst to do a least squares fit. This method produces a transfer function in polynomial form. The curve fit modeled the first two flexible poles well and produced an eighth order polynomial. See Figure 5.6.

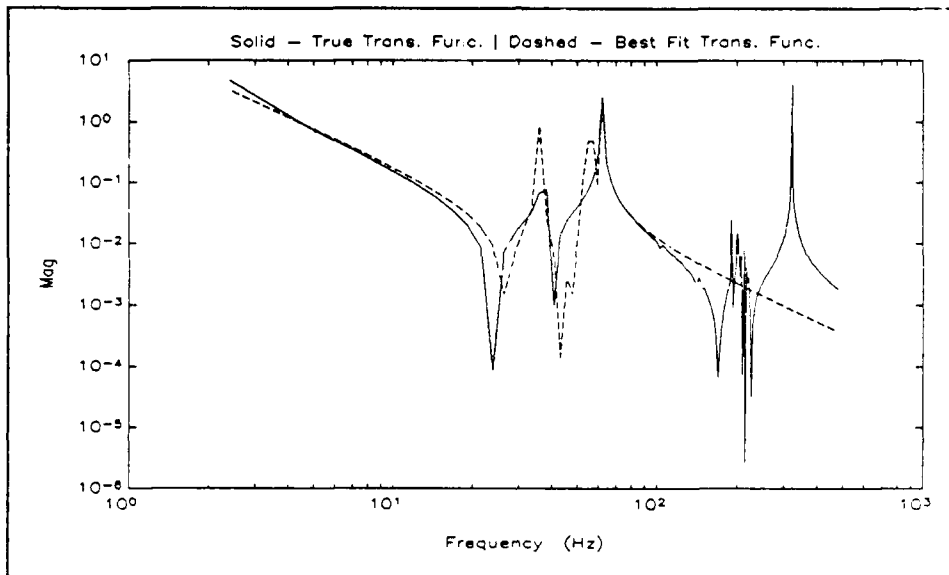


**Figure 5.6** 8th Order Curve Fit Using Ansys.m to the Frequency Response Data

However, converting from transfer function to state space produced a poorly conditioned (A, B, C, D) representation. It appears the most numerically reliable method for state space design is using the FEM modal analysis presented in Chapter 4.

## 5.2 LQG/LTR DESIGN ON THE GIMBAL

The final A matrix after truncation and reduction is 8 x 8 in size. The state weighting selected for the colocated system is

$$Q_c = \text{diag}(10^6 \ 10^6 \ 10^3 \ 10^3 \ 10^2 \ 10^2 \ 10 \ 10),$$

and for the non-collocated sytem is

$$Q_c = \text{diag}(10^{5.5} \ 10^{5.5} \ 10^3 \ 10^3 \ 10^2 \ 10^2 \ 10 \ 10)$$

For both cases, the noise intensity at the input was modeled as

$$Q_o = 10^7.$$

The closed loop bandwidth for the LQG designs are shown in Figure 5.6 where the crossover frequency is defined as -3dB below the 0dB axis.

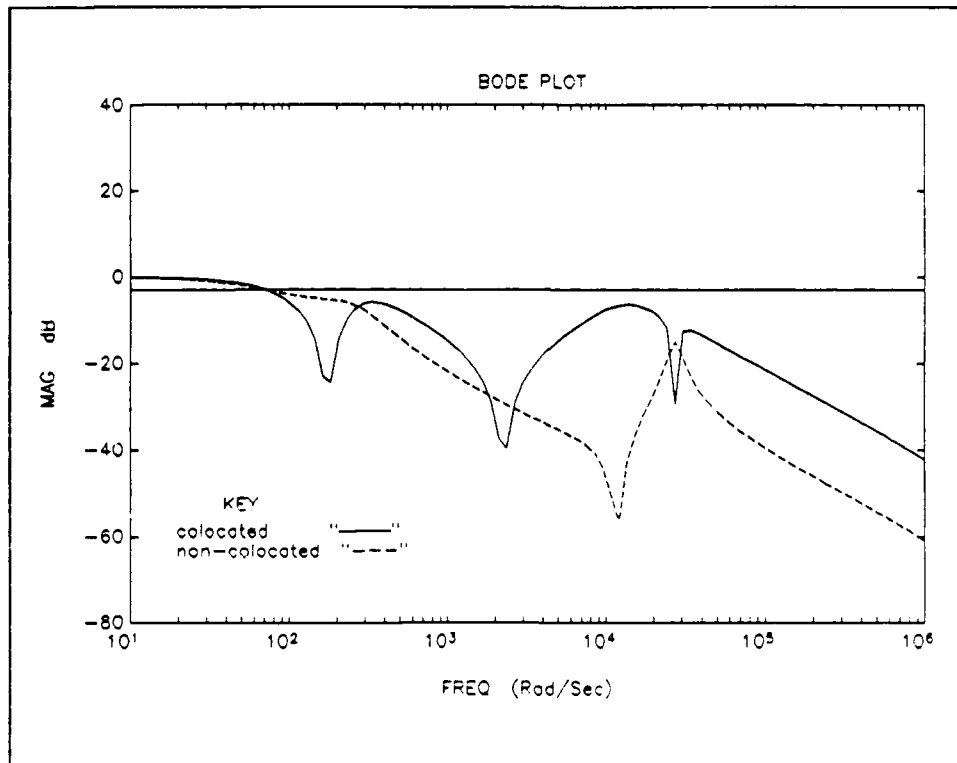


**Figure 5.7** Closed Loop Bandwidths for the Contraves Model

The LQG design without LTR for the colocated case produced a system that went unstable at gain  $k = 5.5$ . The non-colocated system went unstable at  $k = 2.5$ . Interestingly, the LQG design for both systems placed compensator zeros in the RHP. It was not until the fictitious noise value became  $q^2 = 10^9$  did the all the colocated compensator zeros move into the LHP. At this time, the system became very robust and it went unstable at  $k = 25$ . The non-colocated case never gained any robustness after LTR. Its compensator zeros remained in the RHP for all fictitious noise values. See the results in Table A.3 in appendix A. The loop transfer recovery plots and

the root locus plots for the colocated and non-colocated cases are shown on the following pages.

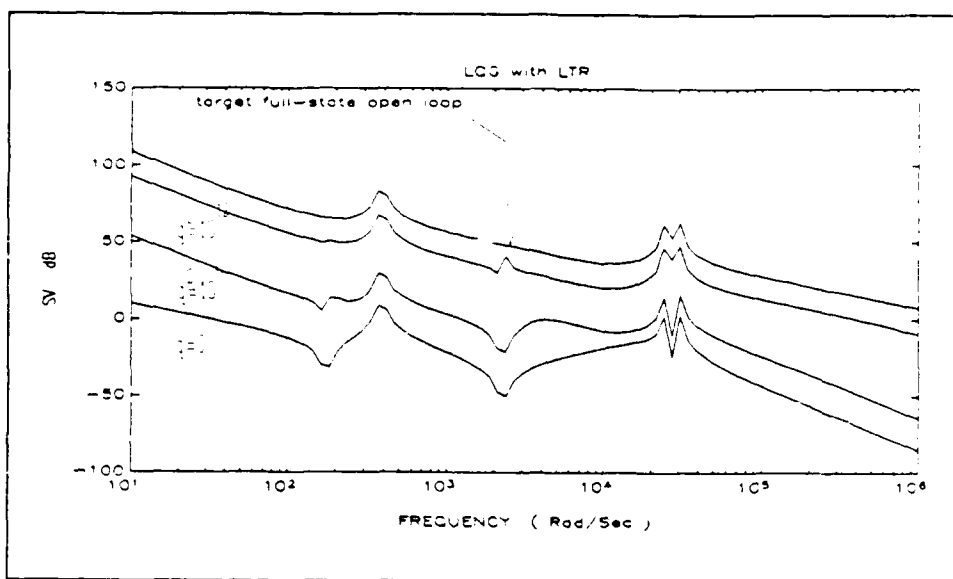


Figure 5.8 LTR for the Colocated System

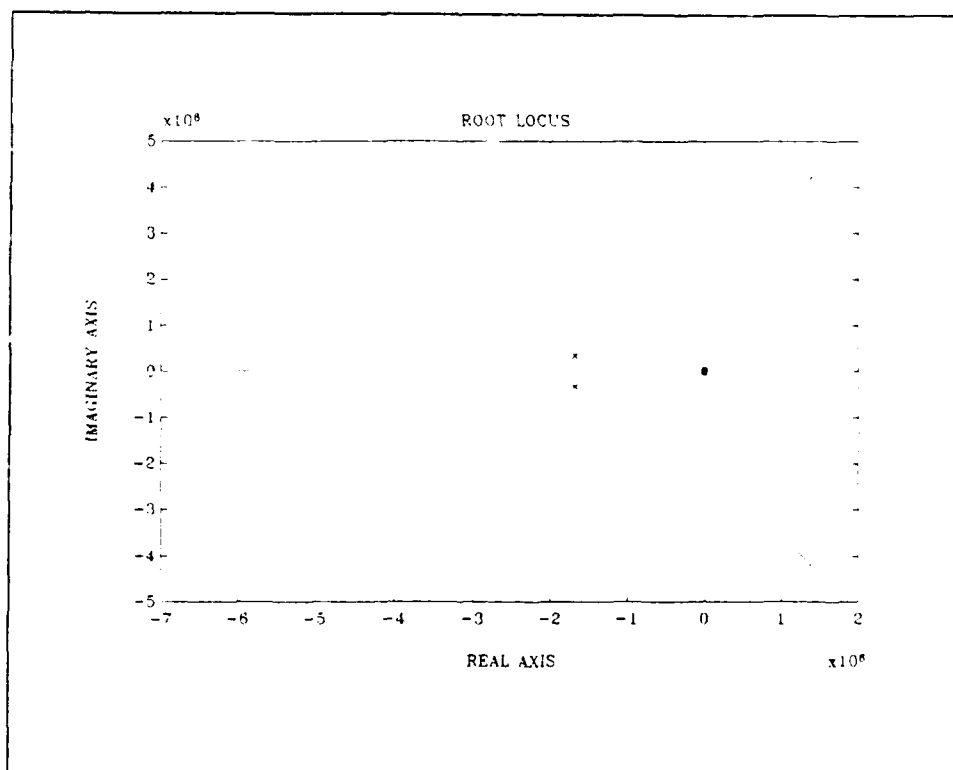


Figure 5.9 Root Locus for the LQG Design with LTR for the Colocated System

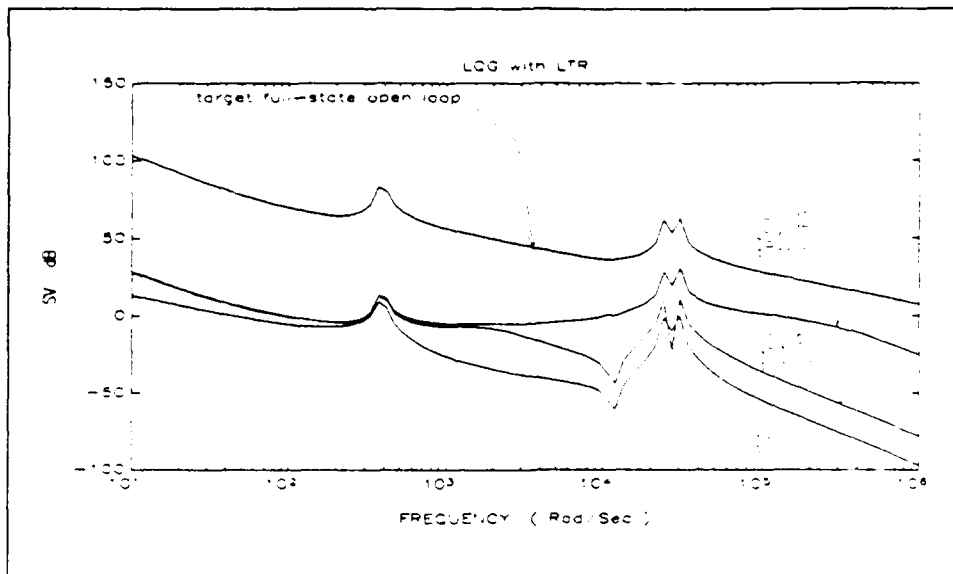


Figure 5.10 LTR for the Non-colocated System

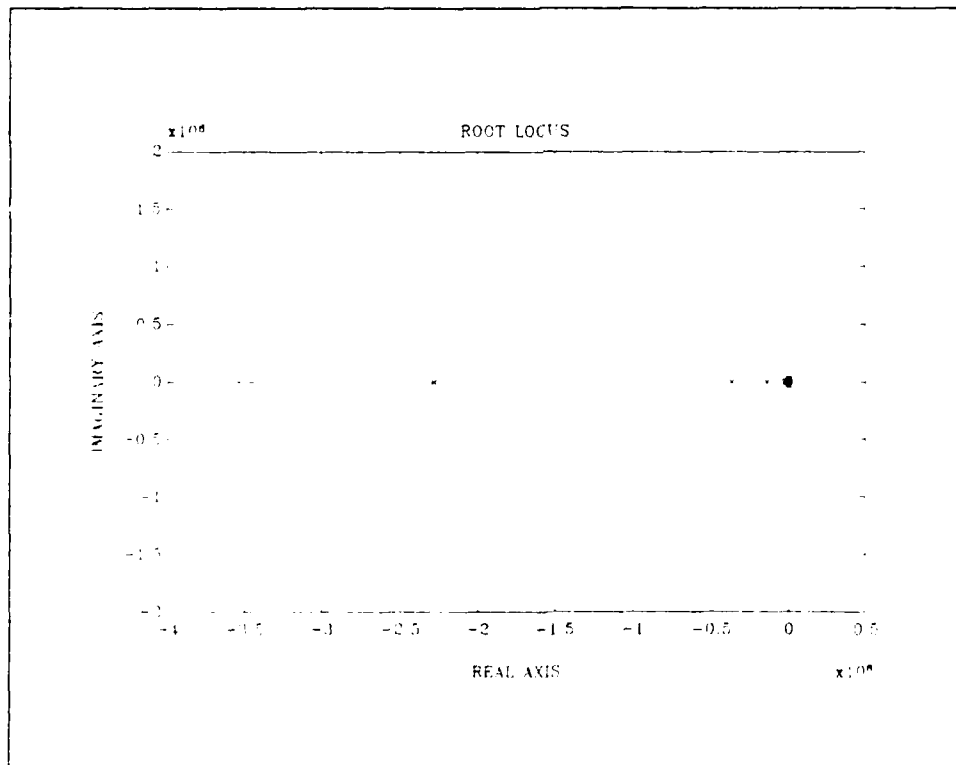


Figure 5.11 Root Locus for the LQG Design with LTR for the Non-colocated System

### 5.3 STEP RESPONSE

The step response of Figure 5.12 shows the colocated and non-colocated systems having similar rise times. Both systems have good damping of its poles with the colocated showing a small fluctuation due to its zero on the imaginary axis. The non-colocated system because it has RHP zeros has the initial negative rise in its step reponse.

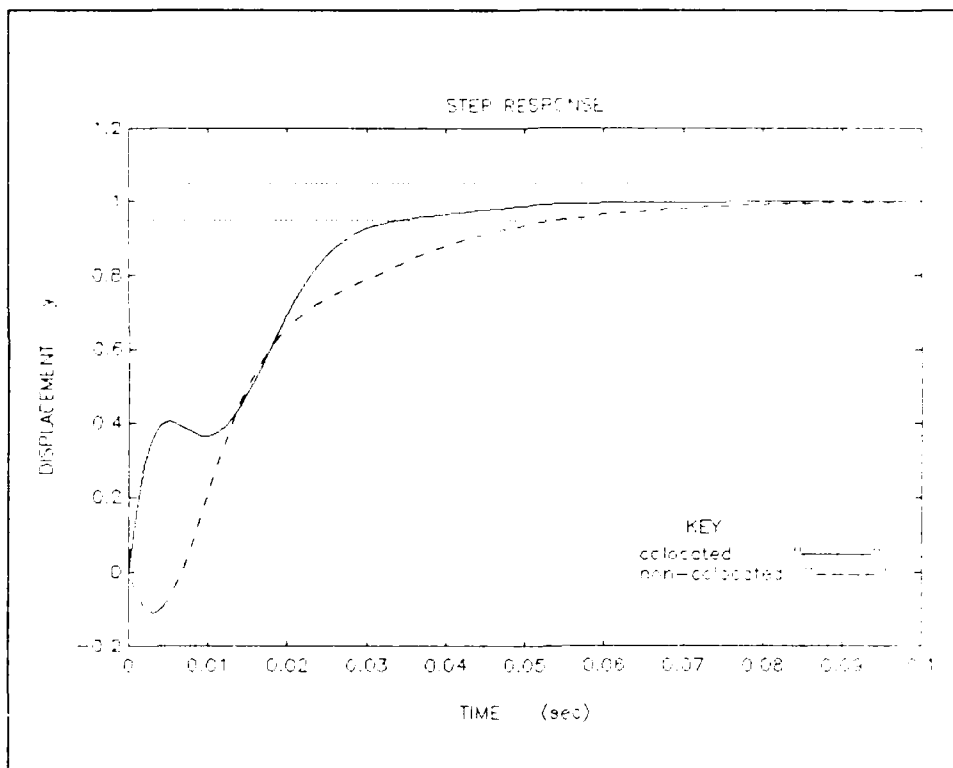


Figure 5.12 Step Response of the Contraves Gimbal

#### 5.4 CONCLUSION

The non-colocated system since it was non-minimum phase could not recover any robustness with LTR. On the other hand, the colocated system after sufficient fictitious noise was added at the plant input increased its robustness. See Table A.3 in Appendix A.

The RMS noise responses for the colocated system was generally larger than the non-colocated system due to the larger  $Q_c$  weighting matrix used. The unit step input response revealed the negative rise expected from non-minimum phase systems for the non-colocated case. Both rise times were the similar and both had good damping.

Some modeling inaccuracies were introduced by modal truncation of the very large system to only the first five modes. Even then, one of the modes proved to be unobservable and had to be removed from the analysis. More analysis with higher order models might be needed to more accurately model the system.

## VI. CONCLUSIONS AND RECOMMENDATIONS

### 6.1 SUMMARY

Chapter II introduced the three element lumped mass model to illustrate basic principles of pole/zero patterns associated with different cases of sensor and actuator locations. The colocated system (sensors and actuators at the same location) has the desirable property of alternating poles and zeros on the imaginary axis. This pole/zero pattern makes it easy to stabilize the system with a simple lead compensator. The non-colocated system could not be stabilized with a lead compensator. Because the three element model is a single motion DOF system, it did not have any RHP zeros. But, it exhibited non-minimum phase like behavior. The non-colocated system required a higher order controller to stabilize it.

Chapter III introduced the LQG/LTR theory used to design the higher order controller for the non-colocated system. Despite large fictitious noise added, loop recovery was limited and marginally successful only at low frequencies. It maintained its high frequency roll-off characteristic of a non-minimum phase system.

To show RHP zeros of a non-minimum phase system, Chapter IV introduced the FEM and the ten element transverse beam. This model exhibited the RHP zeros for the non-colocated case. As expected of a non-minimum phase system, LTR had little effect on improving the robustness in comparison to the colocated system. Because the LTR theory relies on placing the poles of the Kalman filter at the plant's zeros, the RHP zeros make this impossible to accomplish. For the colocated system, LQG design without LTR was sufficient to make it very robust. However, LTR made the system much more robust as it approached the robustness of the target full-state loop.

Chapter V designed the LQG/LTR controllers for the Contraves gimbal. The final results were similar to the ten element beam. LTR made the colocated system more robust, although the robustness did not increase linearly. Of course, the non-colocated system which had RHP zeros had unsuccessful LTR.

This finite element model was much more complex than the beam; therefore, modal truncation did not model one of the system's flexible poles at 250 rad/sec. However, this flexible pole was above the design bandwidth of 100 rad/sec. The author considered the system to be accurate enough for design comparisons.

Interesting observations were made concerning the LQG/LTR controllers. LQG design is helped by LTR because as the fictitious noise is increased, the compensator poles move

toward the open loop plant zeros to notch them out. The Kalman filter accomplishes this task since its closed loop poles  $(A - K_f C)$  at high  $q^2$  values moves to the plant zeros. On the other hand, the compensator zeros move toward the stable poles of the closed loop regulator  $(A - BK_c)$ . Thus, during compensated feedback the plant poles move to the compensator zeros which recovers the robustness of the full-state regulator.

The two designs are compared in Table 6.1. The following were used as criteria:

A. Robustness

1. Gain at which the root locus goes into the RHP
2. Whether full recovery to the target full state loop is achieved
3. Alternating poles and zeros indicating whether a system can be easily stabilized

B. Performance

1. Bandwidth
2. Step response
  - settling time
  - ringing
  - initial negative response or no response
3. Damping
4. RMS noise response

### C. Designability

1. RHP compensator poles
2. High frequency roll off
3. State weighting required

**Table 6.1 Comparison of Colocated and Non-colocated Systems**

<u>COLOCATED DESIGN</u>	<u>NON-COLOCATED DESIGN</u>
A.1: Robust to gain variations	Not robust to gain variations
A.2: LTR is possible over a large bandwidth	LTR is not achieved, especially at high frequency
A.3: Has alternating poles/zeros	No alternating pattern
B.1: Lower bandwidth achievable	Higher bandwidth achievable
B.2: - Faster settling time - Ringing - n/a	- Slower settling time - No ringing - Initial negative response
B.3: Poorly damped poles	Poles damped well
B.4: Higher RMS response	Lower RMS response
C.1: Compensator can have RHP poles for both systems	
C.2: No high frequency roll-off	High frequency roll-off
C.3: Larger state weighting matrix required to match bandwidth	Smaller state weighting

## 6.2 CONTRIBUTION

It appears each system has its own advantage. The colocated system is very robust and can handle large gain variations. But, the colocated system for a given state weighting matrix can not achieve the same bandwidth the non-colocated system can. If performance was more important than robustness, the non-colocated system may be desired. Of course, one has to live with the initial negative response of a non-minimum phase system. Therefore, the control engineer can determine whether to go with colocation or non-colocation depending on the specifications that are required.

## 6.3 RECOMMENDATION FOR FURTHER STUDY

To continue to the research on the effects of colocation and non-colocation of sensors and actuators, several other factors need to be evaluated. The selection of the state weighting matrix,  $Q_c$ , seems to have a major influence on the bandwidth, damping, and the noise. Several references should be investigated further in selecting the weighting matrices. Major Michael DeLorenzo presents an algorithm for efficient weight selection techniques in Reference 2. One more source that should be examined is Gunter Stein and Michael Athans paper LOG/LTR Procedure for Multivariable Feedback Control

Design. They also introduce a formal weight augmentation procedure that should be investigated. Further LQG/LTR design iterations should be attempted based on the optimum  $Q_c$  selected.

Second, the noise from the LTR procedures need to be evaluated to see what influence it has on the robustness and to quantify when it drives systems unstable. Third, more different modal truncations need to be tried on the Contraves gimbal to model all the low frequency poles. However, it may require additional sensors to observe the modes that are not observable with a rotational sensor. Thus, further research on the effects of colocation and non-colocation should be done on multi-input and multi-output systems.

## Appendix A: LQG/LTR Design Results

**Table A.1** LQG/LTR Design Results of the Three Element Model

$q^2$	RHP K(s) poles*		RHP K(s) zeros*		RMS Response		Root Locus gain k**	
	co	non	co	non	co	non	co	non
0	no	no	no	yes	1.00	1.14	30	1.75
$10^3$	no	no	no	yes	1.25	1.02	30	1.75
$10^6$	no	yes	no	no	3.51	2.46	17	1.25
$10^9$	no	yes	no	no	7.46	4.06	6.5	1.5
$10^{12}$	no	no	no	no	11.27	3.54	8.0	1.5
$10^{15}$	no	no	no	no	12.41	3.00	28.5	2.0
$10^{18}$	no	no	no	no	12.61	2.66	30	2.75
$10^{20}$	no	no	no	no	12.61	2.44	30	4.0

Note:

$q^2$  = fictitious noise value

\* = "yes" means compensator has RHP poles or zeros for the colocated or non-colocated systems

\*\* = the gain value of the closed loop compensator and plant when its eigenvalues(the poles) goes into the RHP

**Table A.2** LQG/LTR Design Results of the Ten Element Beam

$q^2$	RHP K(s) poles*		RHP K(s) zeros*		RMS Response		Root Locus gain k**	
	co	non	co	non	co	non	co	non
0	no	no	no	yes	4.8	156	43	2
$10^3$	no	no	no	yes	5.8	1.5i	36	2
$10^6$	no	no	no	yes	6.1	582	34	2
$10^9$	no	no	no	yes	10.8	8.6e4	15	2
$10^{12}$	no	no	no	yes	12.3	530	37	2
$10^{15}$	no	no	no	yes	12.4	9.3e3	199	2
$10^{18}$	no	no	no	yes	12.4	4.6e3i	1100	2

**Table A.3** LQG/LTR Design Results of the Contraves Gimbal

$q^2$	RHP K(s) poles*		RHP K(s) zeros*		RMS Response		Root Locus gain k**	
	co	non	co	non	co	non	co	non
0	no	no	yes	yes	40.9	39.1	5.5	2.5
$10^3$	no	no	yes	yes	42.3	41.7	7	2
$10^6$	no	no	yes	yes	95.0	67.5	3	2
$10^9$	no	no	no	yes	239	157	25	2
$10^{12}$	no	no	no	yes	509	247	8	2
$10^{15}$	no	no	no	yes	885	389	6.5	2
$10^{18}$	no	yes	no	yes	1044	3209	17	2

## Appendix B: ANSYS FEM Files

### Ten Element Beam Model

```
/PREP7
/TITLE, Free-Free Beam with E = 1000
```

```
KAN,2
KAY,2,5
KAY,3,1
```

```
/COM NODE DEFINITIONS
```

```
CSYS, 0
```

```
N, 1, 0., 0., 0.
N, 2, 300., 0., 0.
N, 3, 600., 0., 0.
N, 4, 900., 0., 0.
N, 5, 1200., 0., 0.
N, 6, 1500., 0., 0.
N, 7, 1800., 0., 0.
N, 8, 2100., 0., 0.
N, 9, 2400., 0., 0.
N, 10, 2700., 0., 0.
N, 11, 3000., 0., 0.
```

```
/COM Real constant table
```

```
RSIZE, 10
R, 1, 15000., 1.25E+07, 100.
```

```
/COM Material properties
```

```
MP,EX, 1, 1000
MP,NUXY, 1, 3.000000E-01
MP,DENS, 1, 7.8330000E-09
MP,ALPX, 1, 0.000000E+00
```

```
/COM Element type table
```

```
ET, 1, 3, 0, 0, 0, 0, 0, 0
```

```
/COM ELEMENT DEFINITIONS
```

```
TYPE, 1 $ REAL, 1 $ MAT, 1
```

EN, 1, 1, 2  
EN, 2, 2, 3  
EN, 3, 3, 4  
EN, 4, 4, 5  
EN, 5, 5, 6  
EN, 6, 6, 7  
EN, 7, 7, 8  
EN, 8, 8, 9  
EN, 9, 9, 10  
EN, 10, 10, 11

DDELE, 1, ALL, 11

/COM NODAL DISPLACEMENT RESTRAINTS

D,all,ux,0  
D,all,rotz,0

/COM Load set 1

M,1,uy  
M,11,uy

TOTAL,4  
ITER,4,1,1

/COM NODAL FORCES

F, 11, FY, 1.

FREQ,100,25000  
SV,,1,1  
SVTYPE,1

LWRITE  
AFWRITE  
FINISH  
/OUTPUT,mode4E,out  
/EXE  
/INPUT,27  
FINISH

# Contraves P52F Gimbal

## C\*\*\* PARAMETRIC 52T PARAMETERS

### C\*\*\* PAYLOAD

\*SET,PWT,200 \* "PAYLOAD WEIGHT , POUNDS"  
\*SET,PCG,18 \* CG ABOVE MOUNTING SURFACE  
\*SET,ELAC,1200 \* DEG/SEC^2  
\*SET,AZAC,1200 \* DEG/SEC^2  
\*SET,RINT,54 \* RADIUS TO INTERFACE SURFACE

### C\*\*\* INTERFACE PLATE

\*SET,D1,25 \* WIDTH  
\*SET,D2,25 \* "LENGTH , AZ AXIS DIRECTION"  
\*SET,T1,1.25 \* THICKNESS  
\*SET,D3,20 \* THRU HOLE DIA

### C\*\*\* INNER GIMBAL

\*SET,M1,2 \* MATERIAL STEEL=1 ALUMINUM=2 CAST  
IRON=3  
\*SET,D4,4 \* NARROW SECTION THICKNESS  
\*SET,D8,10 \* THICK SECTION THICKNESS  
\*SET,T2,0.3125 \* WALL THICKNESS  
\*SET,D5,11 \* HALF WIDTH  
\*SET,D6,42 \* CL TO AZ HUB  
\*SET,D7,5 \* HUB HALF HEIGHT

### C\*\*\* CALCULATED

\*SET,RI1,31.156 \* INNER RADIUS BASED ON WIDTH (PLATE  
CL)  
\*SET,RI2,45.156 \* INNER RADIUS BASED ON HEIGHT  
\*SET,RI,31.156 \* LESSER OF ABOVE  
\*SET,RO,25.918 \* OUTER RADIUS  
\*SET,Z1,11 \* Z COORD OF RI  
\*SET,X1,18.5 \* X COORD OF RI  
\*SET,Z2,19.926 \* Z COORD OF RO  
\*SET,X2,27.457 \* X COORD OF RO

### C\*\*\* AZIMUTH ACTUATOR

\*SET,D50,1.968 \* SHAFT OUTSIDE RADIUS UNDER RINGFEDER  
\*SET,D51,0.750 \* SHAFT WALL  
\*SET,D53,3.125 \* BEARING OUTER RADIUS  
\*SET,D54,6.300 \* ENDPLATE OUTER RADIUS  
\*SET,T50,2.000 \* ENDPLATE THICKNESS

\*SET,D55,4.520 \* STATOR BORE  
 \*SET,D56,1.950 \* STATOR LENGTH  
 \*SET,YAX,2E+06 \* 1/2 HERTZIAN AXIAL BEARING STIFFNESS  
 \*SET,YRAD,4E+06 \* 1/2 HERZIAN RADIAL STIFFNESS

C\*\*\* CALCULATED

\*SLT,AA,0.273 \* 4 BEAM BEARING AREA  
 \*SET,AIYY,0.073 \* 4 BEAM BEARING INERTIA  
 \*SET,D57,48.8 \* INNER ENDPLATE LOCATION  
 \*SET,D58,55.270 \* OUTER ENDPLATE LOCATION

C\*\*\* OUTER GIMBAL

\*SET,M2,2 \* MATERIAL STEEL=1 ALUMINUM=2 CAST  
 IRON=3  
 \*SET,T60,0.313 \* GIMBAL WALL  
 \*SET,T61,0.750 \* HUB WALL  
 \*SET,D61,5.000 \* GIMBAL DEPTH AT YAW HUB (YAW AXIS DIR)  
 \*SET,D62,5.000 \* GIMBAL DEPTH AT CORNER  
 \*SET,D63,4.500 \* WIDTH OF PITCH ARMS  
 \*SET,D65,2.000 \* SPACE BETWEEN TOP/BOT PLATE AND YAW HUB  
 \*SET,D67,6.000 \* HALF HEIGHT AT CORNER  
 \*SET,D68,6.000 \* HALF HEIGHT AT PITCH HUB  
 \*SET,D69,60.000 \* INSIDE HALF LENGTH  
 \*SET,D80,48.000 \* INSIDE HALF LENGTH TO CORNER  
 \*SET,D71,3.937 \* RINGFEDER OUTER RADIUS  
 \*SET,D72,6.000 \* HALF WIDTH OF PITCH HUB  
 \*SET,D73,2.800 \* OUTER GIMBAL TO INBOARD PITCH BEARING  
 \*SET,D74,5.000 \* BEARING-BEARING  
 \*SET,D75,3.000 \* PITCH ACTUATOR SHAFT OUTER RADIUS UNDER  
 RF  
 \*SET,D76,2.000 \* SHAFT WALL

C\*\*\* CALCULATED

\*SET,D60,47.036 \* INNER PLATE LOCATION CL  
 \*SET,D64,6.675 \* AZIMUTH HUB OUTER RADIUS CL  
 \*SET,D66,8.831 \* MODEL HEIGHT  
 \*SET,D70,51.724 \* OUTER PLATE MODEL LOCATION AT YAW HUB  
 CL

C\*\*\* ELEVATION BEARINGS

\*SET,PAX,2E+07 \* 1/2 HERTZIAN  
 \*SET,PRAD,1E+07 \* 1/2 HERTZIAN  
 \*SET,D77,1.000 \* BEAM AREA  
 \*SET,D78,1.2667 \* BEAM IYY

C\*\*\* END PARAMETERS

/PREP7

/TITLE,     PARAMETRIC 52T ELEVATION MODES     P52

KAN,2  
KAY,2,5  
KAY,3,5

ET,1,63  
ET,2,16

ET,3,21,,,2  
ET,4,4

C\*\*\*   DEFINE COORDINATE SYSTEMS

K,1001  
K,1002,1  
K,1003,,1  
K,1004,,,1  
CSKP,11,1,1001,1003,1004 \*ROLL AXIS  
CSKP,12,1,1001,1004,1002 \*PITCH AXIS  
CSKP,13,1,1001,1002,1003 \*YAW AXIS  
CSYS

C\*\*\*   MATERIALS

EX,1,29E6       \*STEEL  
DENS,1,.00088  
NUXY,1,.3

EX,2,1E7        \*ALUMINUM  
DENS,2,.0003  
NUXY,2,.3

EX,9,10E6       \*MASSLESS  
DENS,9,0  
NUXY,9,.3

EX,3,26E6       \*CAST IRON  
NUXY,3,.16  
DENS,3,.0008

**The geometric data is omitted for brevity**

**The complete P52F.DAT file is on disk with Professor Brad Liebster**

C\*\*\*   MIRROR MODEL  
ESEL,REAL,2,90

EASE,REAL,92,99

NELE

CSYS

SYMM,3,1000,ALL

EGEN,2,1000,ALL

ESEL,REAL,2,19

EASE,REAL,21,99

NELE

SYMM,2,2000,ALL

EGEN,2,2000,ALL

C\*\*\*

EALL

NALL

MERG,.1

WAVE

CE,1,,313,UX,1,303,ROTZ,D53

CE,2,,1313,UX,1,1303,ROTZ,D53

CE,3,,2313,UX,1,303,ROTZ,-D53

CE,4,,3313,UX,1,1303,ROTZ,-D53

M,301,ROTZ

M,303,ROTZ

M,1301,ROTY

M,1303,ROTY

TOTAL,5

C\*\*\* END GAME

CSYS

C\*\*\*

NALL

EALL

TOTAL,100

ITER,1,1,1

C\*\*\* RESTRAIN PITCH SHAFT

KD,154,ROTY  
KD,155,ROTY

C\*\*\* PITCH BEARINGS

CSYS,12  
ESEL,REAL,92  
NELE  
NRSE,X,1,111  
D,ALL,ALL  
EALL  
NALL  
CSYS  
AFWR  
FINI

/INP,27

FINI

/SHO,FILE33,DAT,1

C\*\*\* RENAME FILE33.DAT AT END OF RUN

/POST1

/TIT, PARAMETRIC MEDIUM 52T MODES P52

SET,1,1

/VIE,,1,1,1

/VUP,,X

/TYP,,3

EPLO

/TYP

SET,1,1

PLDI,1

/VIE,,, -1

PLDI,1

/VIE,,,, -1

PLDI,1

/VIE,,1,1,1

SET,1,2

PLDI,1

/VIE,,, -1

PLDI,1

/VIE,,,, -1

PLDI,1

/VIE,,1,1,1

SET,1,3

PLDI,1

/VIE,,, -1

PLDI,1

/VIE,,,, -1

PLDI,1

/VIE,,1,1,1

SET,1,4

PLDI,1

/VIE,,, -1

PLDI,1

/VIE,,,, -1

## APPENDIX C: MATLAB PROGRAMS

```
% SCRIPT FILE LQGD.M
%
% Calculates closed loop LQG for colocated and non-colocated
% systems. Also calculates LTR and closed loop bandwidths.
%
% Must have the following matrices available
%   - a,b, co (colocated c matrix), cn(non-colocated c matrix)
%     and d state space matrices.
%   - w, the frequency values from LOGSPACE.M
%   - no, the noise intensity at the input
%
% Inputs are
%
%   Wc and Wn = diagmx(Q,R)
%               Q.M is available to facilitate inputting the
%               diagonal weighting matrix
%   r = fictitious noise values used in loop transfer recovery
%
% This program assumes V = Q0*eye(n) matrix for Kalman
% filter calculations. Select the most realistic possible.
%
% W. C. Lee, 1-1-91

dim=size(a);dim=dim(1);

[mc,pc]=bode(a,b,co,d,1,w);      % Bode plots of the open loop plant
[mn,pn]=bode(a,b,cn,d,1,w);

clear k
!del graph.met;

for i=1:100    % Runs the menu for up to 100 iterations

if (i~=1)
k=menu('LQGD MENU','LQR colocated iteration','Continue to LTR design',...
      'LQR non-colocated', 'LTR non-colocated', 'Comparison','Exit'); end

if (k==6)
disp('run graphit to get prints from this session')
% clear r dfc dfn Bb Bbn Cb Cbn Db Dbn pcc pc pcn pn MC MN sys
% clear dim xi th sck scko sckn skcno Ab ABn bfc cfc bfn cfn
return

end;

% COLOCATED FULL-STATE REGULATOR DESIGN ITERATION
```

```

if (k==1)

    Wc=input('input Wc = ');
    kc=lqrc(a,b,Wc);
    skc=sigma(a-b*kc, b,co,d,1,w);    % Closed loop LQR

    loglog(w,mc,w,skc),title(['Closed loop LQR - colocated    graph #
',...    int2str(i) ] );
    pause

%meta graph    % puts graphs into graph.met for later printing

end

%    LTR DESIGN

if (k==2)

    sys=[a b;co d];
    xi=no*eye(dim);th=1;    %    Select xi based on individual problem

    skco=20*log10(sigma(a,b,kc,d,1,w));    % SV for open loop LQR
    r=input('input r for loop recovery = ');

    [afc,bfc,afc,dfc]=ltrin(sys,dim,kc,xi,th,r,w,skco);
    kf=bfc;

%    Closed loop K(s)G(s) system

    Ab=[a -b*kc;kf*co a-b*kc-kf*co]; Bb=[b;b]; Cb=[co zeros(co)]; Db=d;
    [mcc,pcc]=bode(Ab,Bb,Cb,Db,1,w);

%loglog(w,mc,w,mcc),title(['Colocated    LQG        closed    loop    graph    #
',int2str(i) ] );

end

%    NON - COLOCATED    LQR DESIGN ITERATION

if (k==3)

    Wn=input('input Wn = ');
    kcn=lqrc(a,b,Wn);
    skcn=sigma(a-b*kcn, b, cn,d,1,w);

    loglog(w,mn,w, skcn),title(['Closed loop LQR for non-colocated
graph # ',... int2str(i)] );
    pause

% meta graph

```

end

% NON-COLOCATED LTR DESIGN

if (k==4)

```
sys=[a b;cn d];
xi=no*eye(dim);th=1;      % select xi based individual problem
```

```
skcno=20*log10(sigma(a,b,kcn,d,1,w));
r=input('input r for loop recovery = ');
```

```
[afn,bfn,cfn,dfn]=ltrin(sys,dim,kcn,xi,th,r,w,skcno);
kfn=bfn;
```

```
Abn=[a -b*kcn; kfn*cn a-b*kcn-kfn*cn]; Bbn=[b;b]; Cbn=[cn
zeros(cn)];
Dbn=d;
```

```
[mcn,pcn]=bode(Abn, Bbn, Cbn,Dbn,1,w);
%loglog(w,mn,w,mcn),title(['Non-Colocated LQG closed, graph # ',int2str(i)
] );
```

end

% Compare closed loop bandwidth

if (k==5)

```
MC=20*log10(mcc/mcc(1) ); MN=20*log10(mcn/mcn(1) );
w1=[min(w) max(w)];
semilogx(w,MC,'-',w,MN,'--',w1,-3*ones(w1),w1,60*ones(w1)) title('
BODE PLOT');
```

```
xlabel('FREQ (Rad/Sec)')
ylabel('MAG dB')
text(.2,.3,'KEY','sc')
text(.15,.26,'colocated "____"', 'sc')
text(.15,.23,'non-colocated "----" ', 'sc')
```

```
pause
meta graph
```

end

end % goes with for i=1:100 on top

# LTRIN.M

```
function [af,bf,cf,df,svl] = ltrin(sys,dim,Kc,xi,th,r,w,svk)

% My modified LQG/LTR program to calculate loop transfer recovery
% and compare open loop SV for LQR and LTR
%
% [af,bf,cf,df,svl] = ltrin(sys,dim,Kc,xi,th,r,w,skc)
%
% LQG/LTR at inputs of the plant, such that the LQG loop TF
% will converge to LQSF's loop TF as the plant noise goes to INF:
%
% 
$$GKc(Is-A+B*Kc+Kf*C) Kf \xrightarrow{-1} Kc(Is-A) B \quad (\text{as } r \rightarrow \text{INF})$$

%
% Inputs: sys -- system matrix,
%          dim -- no. of states
%          Kc -- LQR gain,
%          skc -- SV of (Kc inv(Is-A)B) *** Must be input as dB ***
%          w -- frequency points (rad/sec)
%          xi -- plant noise intensity, taken as identity
%          th -- sensor noise intensity, taken as identity
%          r -- a row vector containing a set of recovery gains
%
% Outputs: svl -- singular value plots of all the recovery points
%           (af,bf,cf,df) -- final state-space controller
%           where bf=Kf and cf=Kc
% -----%
```

```
nq = length(r);
[A,B,C,D] = sys2ss(sys,dim);
[md,nd] = size(D);

for i = 1:nq
    disp(' ')
    disp([' LQG/LTR ---> recovery gain = ' num2str(r(1,i)) ' ..']);
    xi = xi + r(1,i)*B*B';
    qrnc = diagmx(xi,th);
    Kf = lqrc(A',C',qrnc);
    Kf=Kf';

    af = A - B*Kc - Kf*C;
    bf = Kf;
    cf = Kc;
    df=D;
% df = zeros(size(Kc)*[1;0],size(Kf)*[0;1]);

    [al,b1,c1,d1] = series(af,bf,cf,df,A,B,C,D);
    sv = sigma(al,b1,c1,d1,1,w); sv = 20*log10(sv);
```

```

        if i == 1
            sv1 = sv;
        else
            sv1 = [sv1;sv];
        end
    end

end      % for I=1:NQ

semilogx(w,svk,w,sv1)

title('LQG with LTR')
xlabel('FREQUENCY ( Rad/Sec )')
ylabel('SV   dB')
text(.17,.88,'target full-state open loop ','sc')
pause
meta graph

disp('(run graphit to get print.  Sent to LN03)')

%
% ----- End of LTRY.M -- RYC

```

# ROOTPLOT.M

```
function r=rootplot(a,b,c,d,kc,kf,alpha,zero)

% ROOTPLOT  R=Rootplot(A,B,C,D,Kc,Kf,alpha,zero)
%
%      alpha - gains on the output matrix c
%      zero  - the zeros from tzero with large ones omitted
%
%      Same as RLOCUS except that the roots are automatically
%      plotted and crosshairs appear for determining the gain
%      corresponding to a desired closed loop pole location.
%      Once the crosshairs are positioned near a pole on the
%      screen, hitting carriage return results in the calculation
%      and display of the gain corresponding to the nearest
%      closed loop pole. In addition all: the closed loop poles,
%      their natural frequencies and damping factors
%      corresponding to that gain are displayed.
%
%  B.S. Liebst, 6-1-88
%  W. C. Lee, 1-1-91

poles=eig(a);
pr=real(check(poles));
pi=imag(check(poles));
zr=real(zero);
zi=imag(zero);

r=[];

if(nargin~=8);

    for i=1:length(alpha)

        cstar=alpha(i)*c;
        abig=[a -b*kc;kf*cstar a-b*kc-kf*c];

        rt=eig(abig);
        r=[r;rt'];

    end

else
    error('Incorrect number of input arguments')
end

j=sqrt(-1);is=0;km=1;

plot(real(r),imag(r),'.','pr,pi','x',zr,zi,'o')
title(' ROOT LOCUS')
xlabel('REAL AXIS')
```

```

ylabel('IMAGINARY AXIS')

for ic=1:500
    is=is+1;

    if(is>1),km=menu('ROOTNEW  MENU','Show root locus','Exit');end

    if(km==2),return,end

    shg

    [xr,yr]=ginput(1);
    rq=(xr+j*yr)*ones(r);
    rq=r-rq;
    [y,i1]=min(rq);
    [y,i2]=min(y);

    i1=i1(i2);
    kq=alpha(i1);

    clc
    disp('Gain, alpha = ')
    disp(kq)

    rq=r(i1,:);
    [wn,z]=damp(rq);

    disp('      cl. loop roots          wn          zeta')
    disp(' ')
    disp([rq+j*zeros(rq) wn z])
    disp('Hit carriage return to continue')
    pause

end

```

# NOISE.M

```
function [Qx]=noise(a,b,c,kc,kf)

% NOISE    [Qx] = noise(a,b,c,kc,kf)
%
%    Solves the Lyapunov equation for output noise RMS value
%
%     $AX + XA^T + BVB^T = 0$ 
%
%    assumes that V is identity
%

Ab=[a -b*kc;kf*c a-b*kc-kf*c];    % Closed loop K(s)G(s) system
Bb=[zeros(kf);kf];

X=lyap(Ab,Bb*Bb');
diag(X)

Cb=[c zeros(c)];
Qx=Cb*X*Cb';
```

# STEPP.M

```

function stepp(a,b,co,cn,d,kc,kcn,time,type)

% STEPP stepp(a,b,co,cn,d,kc,kcn,time,type)
%
% Calculates step response for closed loop full-state regulator
%
% time needs to be in small enough steps to cover the poles
%
% type = 1 plot normalized to steady state value
% type = 2 plot normalized to max value

!del graph.met;1

Yc=step(a-b*kc,b,co,d,1,time);
Yn=step(a-b*kcn,b,cn,d,1,time);

w=[min(time) max(time)]; % set length for faster plotting

if (type==1)
    Yc=Yc/Yc(length(Yc));
    Yn=Yn/Yn(length(Yn));
    plot(time,Yc,time,Yn,w,-.2*ones(w), w,.95*ones(w), ':',...
         w,1.05*ones(w), ':')

% meta graph
% pause

end

if (type==2)
    Yc=Yc/max(Yc);
    Yn=Yn/max(Yn);
    plot(time,Yc,time,Yn,w,.95*ones(w), ':',w,1.05*ones(w), ':',...
         w,-.2*ones(w))

meta graph

end

title('STEP RESPONSE');
xlabel('TIME (sec)');
ylabel('DISPLACEMENT y')
text(.7,.3,'KEY','sc')
text(.65,.26,'colocated "____"', 'sc')
text(.65,.23,'non-colocated "----"', 'sc')
meta graph
pause
disp('run graphit to get prints')

```

## Bibliography

1. Cannon, Robert H., Jr. and Dan E. Rosenthal, "Exeriments in Control of Flexible Structures with Noncolocated Sensors and Actuators", Journal of Guidance. 7:546-553 (Sept-Oct 1984)
2. DeLorenzo, Major Michael L. "Sensor and Actuator Selection For Large Space Structure Control". Studenet Report. Air Command and Staff College, Air University, Maxwell AFB, AL. June 1988. (AD-A194912)
3. Gervarter, W. B. "Basic Relations for Control of Flexible Vehicles", AIAA Journal. 8: 666-672 (April 1970).
4. Kopf, E. H., T. K. Brown, and E. L. Marsh, "Flexible Stator Control on the Gailileo Spacecraft", AAS Paper 79-161, Provincetown, MA, June 1979.
5. Kwakernaak, H. and R. Sivan. Linear Optimal Control Systems New York: Wiley-Interscience, 1972.
6. Maciejowski, J. M. Multivariable Feedback Design. Workingham, England: Addison-Wesley Publishing Company, 1989.
7. Martin, Gary D. On the Control of Flexible Mechanical Systems, Ph. D. dissertaiton, Dept of Aeronautics and Astronautics, Standford University, Standford, CA. May 1978 (SUDAAR 511)
8. Meirovitch, Leonard. Elements of Vibration Analysis. New York: McGraw-Hill Book Company, 1986.
9. Meriovitch, Leonard. Analytical Methods in Vibrations. New York: Macmillian Publishing Co., Inc., 1967.
10. Reid, J. Gary. Linear Systems Fundamentals. New York: McGraw-Hill Book Company, 1983.
11. Ridgely, Brett D. and Siva S. Banda. Introduction to Robust Multivariable Control. AFWAL -TR-85-3102. WPAFB, OH: Control Dynamics Branch, Flight Dynamics Laboratory, September 1985. (AD-A165891)

12. Thomas, H. L. and L. A. Schmit, Jr. "Control Augmented Structural Synthesis with Dynamic Stability Constraints", AIAA Paper 89-1216. April, 1989.
13. Thomson, William T. Vibration Theory and Applications. Englewood Cliffs, N.J.: Prentice-Hall, Inc., 1965.
14. Wie, Bong and Arthur E. Bryson, Jr. "Modeling and Control of Flexible Space Structures", Dynamics and Control of Large Flexible Spacecraft: Proceedings of the Third Symposium, Blacksburg, VA, June 15-17, 1981.